1993ApJ...403..780T

THE ASTROPHYSICAL JOURNAL, 403:780–796, 1993 February 1
© 1993. The American Astronomical Society. All rights reserved. Printed in U.S.A.

ON THE MAGNETIC AND VELOCITY FIELD GEOMETRY OF SIMPLE SUNSPOTS

ALAN M. TITLE, ZOE A. FRANK, RICHARD A. SHINE, THEODORE D. TARBELL, AND KENNETH P. TOPKA
Lockheed Palo Alto Research Laboratory, 3251 Hanover Street, Palo Alto, CA 94304-1191
GÖRAN SCHARMER
Swedish Royal Academy of Sciences, Stockholm Observatory, S-13336 Saltsjöbaden, Sweden
AND
WOLFGANG SCHMIDT
Kiepenheuer-Institut für Sonnenphysik, Schöneckstrasse 6, D-7800 Freiburg im Breisgau, Germany
Received 1992 January 20; accepted 1992 August 6

ABSTRACT

We have observed the disk passage of relatively simple round sunspots using a narrow-band filter and a large format CCD detector and have created magnetograms, Dopplergrams, and continuum images nearly simultaneously. The spectral resolution of the filter (88,000) allows the construction of "spectra" for all points in the field of view. The changing patterns of the line-of-sight magnetic fields with position around the spots and with position of spots on the solar disk show that the mean inclination of the magnetic field increases from 45°–50° to 70°–75° across the penumbra and that there is a fluctuation about the mean of about $\pm 18°$. These inclination changes occur on the scale of the penumbral fibrils. In addition the direction changes are large enough that a substantial fraction of the magnetic field is horizontal (parallel to the solar surface) from the mid to outer penumbra. Our Doppler data show that the Evershed flow tends to occur in the regions where the magnetic field is horizontal. Taken together these observations suggest that the Evershed flow is confined to the regions of horizontal fields, which resolves the old difficulty of nonparallelism of magnetic and flow fields in a sunspot.

We show that a simple sunspot model with azimuthal variations in inclination, but no azimuthal variations of field strength, is free from azimuthal Lorentz forces. The meridional currents which arises from the inclination variations are parallel to the field lines. This suggests that a cylindrically symmetric magnetostatic sunspot model can be perturbed into one with azimuthal variations in inclination with some adjustment in the meridional force balance.

Subject headings: Sun: magnetic fields — sunspots

1. INTRODUCTION

Even a simple round isolated sunspot is very complicated structure (Schröter 1971; Gokhale & Zwaan 1972; Cram & Thomas 1981; Garcia de la Rosa 1987; Kalman 1991). There are intensity inhomogeneities in the umbra and the penumbra, nonsteady outflows in the penumbra (Evershed flows), inward motions of bright points along the bright penumbral fibrils, and various irregular wave motions in the umbra and penumbra. Given the complexity of the intensity, flow, and wave fields, it would be surprising if the magnetic field geometry were not also complex. In this paper we discuss observations of the line-of-sight magnetic and velocity field which suggest that even a simple round spot has a mutually interacting spatially complex magnetic and flow structure.

High-resolution magnetic measurements of sunspots are difficult to obtain. Most birefringent filters are not sufficiently narrow to resolve spectrally the complex profiles of Zeeman sensitive lines in sunspots. Patrol magnetographs are usually optimized for observations outside of spots. High-resolution spectra which measure all four Stokes components with high photometric precision often do not have high spatial resolution. Further, vector magnetic field measurements made with filters and spectrographs are sensitive to errors introduced by telescope polarization. Even if good data are available, the interpretation is complex because the atmosphere of a sunspot is not well understood. In particular the local inhomogeneities of the spot may require very detailed three-dimensional radiative transfer calculations to interpret spectra properly.

The above problems have long been recognized. Observers and theoreticians have generated many clever techniques to infer properties of spots. These have often used the fact that, as a spot moves across the solar disk, the projection of its vector fields on the line of sight changes progressively. In 1908, Evershed (1909) noticed that spot spectra taken with the slit oriented in an east-west direction tended to be sloped with respect to lines of constant wavelength. Center (limb) side spectral elements were blue (red) shifted. These slopes increased as the spot approached the limb; however, slopes were noticeable even for spots which passed quite close to disk center. Evershed inferred that the changing appearance of the spot spectra was due to projection onto the line of sight of nearly radial and nearly horizontal outflow in the penumbra of sunspots. Hale et al. (1918) used spectra of Zeeman triplets taken in right and left circular polarization to measure where the field was perpendicular to the line of sight, which they called the neutral line. By following numerous spots across the disk they were able to generate a mean inclination of the magnetic field as a function of radius.

Hale et al. also observed spots as they crossed the limb in linear polarization at the wavelengths of the π component of Zeeman triplets. Because the linear polarization of the π component is in the direction of the field, this technique directly measured the

© American Astronomical Society • Provided by the NASA Astrophysics Data System

1993ApJ...403..780T

inclination of the field as a function of radius. Taken together, the circular and linear polarization measurements were consistent with a linear increase of the inclination of the magnetic field across the spot with the field normal to the surface at the center of the spot and parallel to the surface at the outer penumbra boundary.

Kinman (1950) elaborated on the earlier projection techniques by making rasters of spectra across individual spots at several disk positions and fitting the observed line of sight flow field to models of simple spot flows. He found that to the accuracy of his measurements the Evershed flow was horizontal with some tendency to be inclined below the horizontal at the outer penumbral boundary. He also found that spots sometimes had a small azimuthal component in their flow field. Maltby (1964) recognized that perfectly symmetrical spots almost never occurred and calculated line-of-sight components of characteristic flow patterns and compared observed flow patterns to his model spots. He established an upper limit of 0.15 km s^{-1} for the vertical component of the Evershed flow and an inclination of the flow to the sunspot normal of at least 84°, or within 6° of surface, at the outer penumbral boundary.

Treanor (1960) developed a polarizing interferometer which allowed determination of the vector field via fringe patterns imposed on spectra. Adam (1971, 1975, 1990) used Treanor's interferometer to measure vector magnetic fields and came to the conclusion that at the outer penumbral boundary the magnitude of the field was about 300 G and the inclination was about 70°. In general, the field inclinations were consistent with a potential field geometry of a shallow buried dipole. Because of the seeing conditions at the Oxford University Observatory the resolution of their spectra was on the order of 4″. Beckers & Schröter (1969) using film spectra taken at Sacramento Peak Observatory did an analysis of Stokes *I*- and *V*-profiles. With 1″ quality data they came to the conclusion that the magnitude of the field strength was about of 1000 G at the outer penumbral boundary and that the inclination of the field with respect to the vertical increased linearly along a sunspot radius and reached 90° at the outer penumbral boundary. Beckers and Schröter also suggested that the magnetic field is stronger and probably more horizontal in the dark penumbral fibrils. Wittmann (1974) also carried out a Stokes profile analysis which agreed with the results of Beckers and Schröter on the inclination of the field but deduced lower field strengths in the outer penumbra.

Recently Lites & Skumanich (1990) reported on a very careful analysis of photoelectric data taken with the High Altitude Observatory Stokes Polarimeter during the decade of the 80's. Their studies of round spots used data with 6″ resolution because of the long integration times required for their desired signal-to-noise ratios. They agreed with Adam on the inclination of the field, but had field strengths in the outer penumbra closer to those of Beckers and Schröter. Further, Lites and Skumanich saw little azimuthal variation in field strength on constant radii. Their results for the vector field of a simple round spot were consistent with the cylindrical symmetric, magnetostatic models of Pizzo (1986, 1990) and Jahn (1989), which are close to the potential field of a buried dipole.

More recently Lites, Scharmer, & Skumanich (1990) have obtained extremely high-resolution spectra of spots using a CCD camera operating at video rates behind the Littrow holographic spectrograph at the Swedish Solar Observatory in La Palma. Often their spectra have a spatial resolution on the order of 0″.3. Although these ultra high-resolution spectra were made without a polarization analyzer, the intensity profiles showed that there is little to no variation of the field strength at a fixed radius on the scale of the penumbral fibrils.

The lack of agreement on the magnetic field inclination in the outer penumbra is in marked contrast to the situation for the Evershed flow, which is generally agreed to be nearly horizontal. However, if the magnetic field is not parallel to the flow field in the highly conducting atmosphere of a sunspot, there is a serious problem in our understanding of the physical processes in the sunspot. Lamb (1975) attempted to interpret the Evershed flows as wave phenomena; but, until now, there has been no satisfactory explanation of how flows and magnetic fields could exist with different geometries in a spot.

In this study we have used sets of filtergrams with spatial resolution of about 0″.5 and spectral resolution of about 88,000 to obtain nearly simultaneous magnetic, Doppler, and continuum intensity data on sunspots in order to clarify the relationship between the Evershed flow and the magnetic field. The data are of very good, but of lesser, quality than the recent spectra of Lites et al. Here we report in detail on two different sets of observations. The first consists of magnetograms and continuum images of a simple round spot on the day before and after disk center passage. The second consists of repeated sequences of filtergrams in the line Fe 5576 Å ($g = 0$) and followed by sequences in both right and left circular polarization in Fe 6302 Å ($g = 2.5$ Zeeman triplet). The wavelength steps are sufficiently close (30 mÅ) to allow the creation of "spectra" for every point in the field of view. The observations are described in § 2. Because of the importance of projection effects, § 3 is devoted to a critique of reliability of the inferences which may be made from line-of-sight and transverse projection of the vector field of a spot. The data analysis methods and results are contained in § 4. In § 5 we examine a simple fluted magnetic field geometry and calculate its current distribution. Finally, in § 6 we summarize our conclusions and suggest an overall structure of the simple sunspot.

2. OBSERVATIONS

The observations were made at the Swedish Solar Observatory Vacuum Tower Telescope on Roque de los Muchachos on La Palma in the Canary Islands (Scharmer 1989) using the engineering evaluation model of the tuneable filtergraph for the Orbiting Solar Laboratory. The observing system is described in Title et al. (1992). From 1988 September 14 through 20 the disk passage of the simple round spot in AR 5168 was monitored. This spot is one of several studied in our program and was chosen for detailed analysis because of the simplicity of the spot, the symmetric crossing of the central meridian, and the quality of the seeing. We have reduced in detail observations made between 8:45 and 9:16 UT on 1988 September 16 (heliocentric angle = 18°.6) and between 15:45 and 15:57 UT on 1988 September 17 (heliocentric angle = 20°.1). These days were just before and just after central meridian passage of the spot. Movies of the disk passage have been made in all our observing wavelengths. The observations of the somewhat more complex spot in AR 6122 were selected because of the line scan observing program used, the central meridian location, and the seeing quality. The filtergrams used for the detailed analysis were taken between 8:04 and 8:59 UT on 1990 June 28 (heliocentric

© American Astronomical Society • Provided by the NASA Astrophysics Data System

1993ApJ...403..780T

angle = 24°.6). In addition to the filtergram movies sequences, we have also created Dopplergram and magnetogram movies which have been reported on separately (Shine et al. 1990). At the time of observation the spot was virtually on the central meridian.

For all these observations the image scale was 1 pixel per 0".162 (120 km on the solar surface), so the field of view was 82" (60,000 km). The filtergram sequence for the simple round spot was a continuous repetition of a cycle of eight images which took about 42 s. Each cycle consisted of: four images for magnetograms, two each in the right and left circular polarization at −60 mÅ from the mean line center of Fe I 6302.5 Å ($g = 2.5$), three images at −700, 0, and +700 mÅ from mean line center of Hα 6562.8 Å, and an image in clean continuum at 6303.2 Å. This sequence allowed the construction of a longitudinal magnetogram and continuum image every 42 s. The data with the best seeing in two adjacent cycles were chosen for the analysis reported here.

The observing sequence on 1990 June 28 was considerably more complex, consisting of a set of filtergrams at 30 mÅ intervals from −120 to +120 mÅ from the line center of Fe 5576 Å ($g = 0$), a similar set taken alternately in right and left circular polarization around the center of Fe 6302 Å, and filtergrams in the continuum near both Fe 5576 Å and Fe 6302 Å. The cycle took 90 s to execute or about 3 s per filtergram. (The increased frame rate in the 1990 observations resulted from software improvements.) The data allowed the construction of arrays of magnetograms and Dopplergrams. Fourier Dopplergrams were created by using the full set of images in Fe 5576 and fitting a cosine matched to the local width of the line at every spatial pixel. Our technique for constructing magnetograms and Dopplergrams is discussed in Title et al. (1992).

For all of the filtergrams the exposure times were adjusted so that the mean exposure level was roughly 60,000 detected photons per pixel (S/N ratio 245). The typical exposure time ranged between 50 and 300 ms. Before the creation of magnetograms and Dopplergrams, all of the filtergrams were corrected for gain and dark current variations and for local flaws in the detector. Separate flat fields were used for each wavelength. The images in both data sets were destretched to remove atmospheric image distortions (Topka, Tarbell, & Title 1986: November 1986) and aligned with respect to each other with an accuracy of about 1/2 pixel (0".08).

3. PROPERTIES OF VECTOR PROJECTION EQUATIONS

A great deal of the analysis of our data depends on interpretation of the projection of local vector fields in a sunspot onto the line of sight. It is therefore useful to examine with some care the inferences that can be made from projection data. Because the diameter of the spot is small compared to the diameter of the Sun, a local vector field in a spot can be described in terms of a rectangular coordinate system that is rotated with respect to the line of sight and centered on the spot. We have used a spot coordinate system with defining unit vectors $\widehat{sx}$, $\widehat{sy}$, $\widehat{sz}$ (see Fig. 1). Our observations are described in another rectangular coordinate system with a common origin at the center of the spot and with defining unit vectors $\hat{x}$, $\hat{y}$, $\hat{z}$. The spot z-axis is in the direction of the surface normal at the center of the spot. Therefore, the angle between the direction of the observing coordinate system z-axis, $\hat{z}$, and the spot z axis, $\widehat{sz}$, is the heliocentric angle, θ. Since the Sun is far from the observer, the line of sight direction, $\hat{z}$, can be either a unit vector from the center of the spot or the center of the Sun to the observer. The spot x-axis direction, $\widehat{sx}$, is in the plane containing the line of sight, $\hat{z}$, and the surface normal, $\widehat{sz}$. These two vectors define the parallel plane. The observing coordinate system x-axis direction $\hat{x}$ is also in the parallel plane. The spot y-axis and the observation plane y-axis are collinear and are perpendicular to the parallel plane.

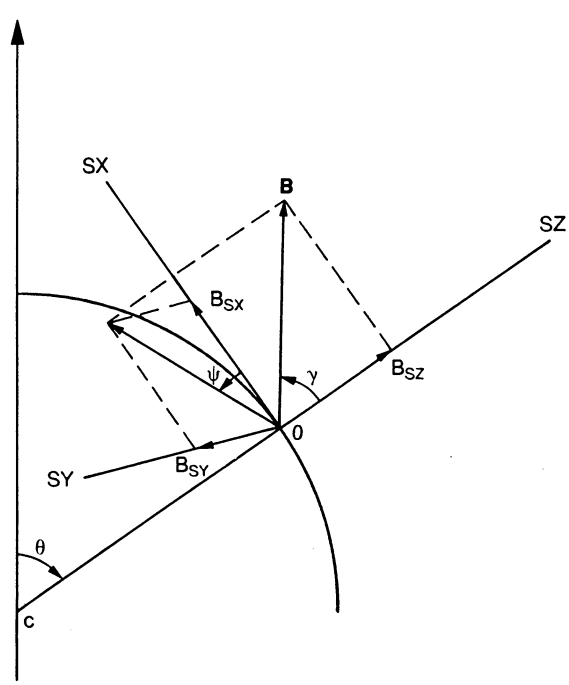

FIG. 1.—Coordinate system for the projection analysis. For clarity only the sunspot axes ($\widehat{sx}$, $\widehat{sy}$, $\widehat{sz}$) are shown. The observing coordinate system and the spot coordinated system have a common origin. The observing coordinate system has the z-axis in direction of the line of sight ($\hat{z}$), the x-axis in the plane determined by $\hat{z}$ and $\widehat{sz}$, and the y-axis collinear with the spot y-axis. In this view both the spot and observing system x-axes are in the plane of the page, and the y-axes are both perpendicular to the page.

© American Astronomical Society • Provided by the NASA Astrophysics Data System

1993ApJ...403..780T

With the above definitions only the components of the spot field in the parallel plane contribute to the line-of-sight component of the field. A vector at radius r and azimuth ψ from the spot center, with inclination to the spot z-axis of γ has a line-of-sight component,

$$V_{\rm LOS}(r_{\rm proj}, \psi_{\rm proj}, \gamma, \theta, \psi + \delta\psi) = V(r, \psi)[\sin\gamma \sin\theta \cos(\psi + \delta\psi) + \cos\gamma \cos\theta] , \quad (1)$$

where $V(r, \psi)$ is the magnitude of the vector $V(r, \psi)$, $(r_{\rm proj}, \psi_{\rm proj})$ is the projected location of the point (r, ψ) on the observation plane, and $\delta\psi$ is measured clockwise from the line connecting the center of the spot and (r, ψ). The location and the projected location are related by

$$r_{\rm proj} = r(\sin^2\psi + \cos^2\psi \cos^2\theta)^{1/2} , \quad (2)$$

and

$$\psi_{\rm proj} = \arctan\left(\frac{\tan\psi}{\cos\theta}\right) . \quad (3)$$

A circle centered on the spot becomes an ellipse on the observation plane with its minor axis in the parallel plane. In most of the discussions here, the vector field will be radial and thus $\delta\psi$ will be zero.

Transverse projections to the line of sight are defined to be along the direction of observation plane x-axis, the parallel component, and along the direction of the observation plane y-axis, the perpendicular component. The parallel component only has contributions from the components in the spot x- and z-axis directions and is

$$V_{\parallel}(r_{\rm proj}, \psi_{\rm proj}, \gamma, \theta, \psi + \delta\psi) = V(r, \psi)[\sin\gamma \cos\theta \cos(\psi + \delta\psi) - \cos\gamma \sin\theta] , \quad (4)$$

while the perpendicular component is

$$V_{\perp}(r_{\rm proj}, \psi_{\rm proj}, \gamma, \psi + \delta\psi) = V(r, \psi)[\sin\gamma \sin(\psi + \delta\psi)] . \quad (5)$$

The magnitude of the transverse component is then just

$$V_{\rm TRAN}(r_{\rm proj}, \psi_{\rm proj}, \gamma, \theta, \psi + \delta\psi) = \sqrt{(V_{\parallel}^2 + V_{\perp}^2)} . \quad (6)$$

In this paper we do not analyze transverse data, however, we have reported on such measurements elsewhere (Topka et al. 1991). We include the discussion of the transverse field patterns because they contribute to our understanding of the distinctive patterns produced by the projection of spot fields. We will discuss the results of the Topka et al. study in our summary.

The transformations from the spot coordinate system to the observation plane coordinate system consists of products and sums of products of trigonometric functions. Therefore, the accuracy with which γ, $\delta\psi$, and $V(r, \psi)$ can be determined can vary greatly depending on the heliocentric angle, θ, and orientation of the vector in the spot coordinate system. Hence, care must be used when inferring properties of the vector field sunspot from the measured projected components. In particular, the determination of the inclinations by means of the neutral line technique is very sensitive to heliocentric position.

Hale introduced the idea of the neutral line. This line occurs in the spot along the path where the field is perpendicular to the line of sight. In our coordinate system if the local vector is in the parallel plane and points in the direction of the limb, that is, it is at $(r, 180°)$ and $\delta\psi$ is zero; then the vector is perpendicular to the line of sight when its inclination, γ, and the heliocentric angle, θ, sum to 90°. In general, there will be line in a spot where the magnetic field in the spot is perpendicular to the line of sight. In principle then, inclinations can be mapped by observing the limb side of the spot and observing as a function of heliocentric position where magnetic field vectors at different radii and ψ have zero projections onto the line of sight.

While the appearance of a neutral line assures that the inclination of the field is at least as great as the complement of the heliocentric angle, unfortunately, it is difficult to learn much more. Consider the case of a cylindrically symmetric spot, the angle subtended by the edges of the reversed field at the penumbral boundary defines a reversal angle, β. The reversal segment (see Fig. 2a)

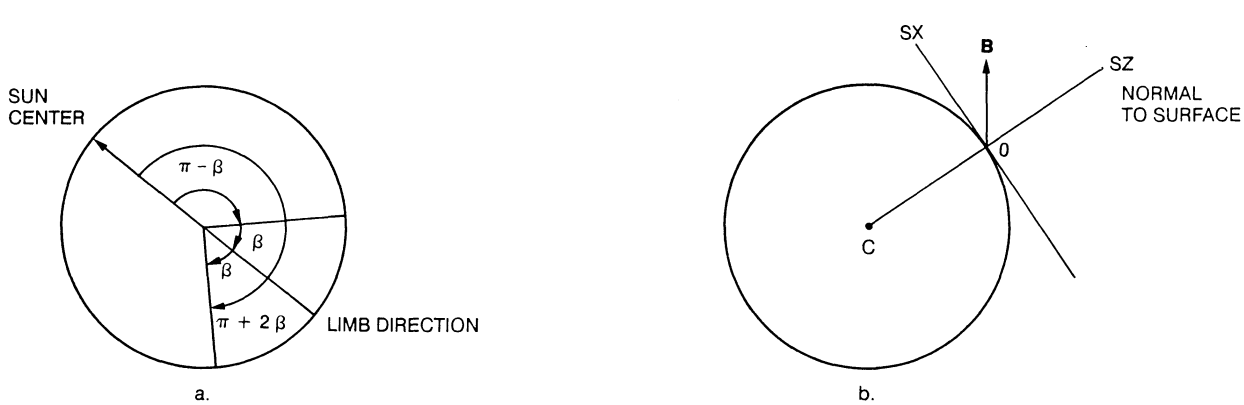

FIG. 2.—Cartoon of simple round spot showing boundary of the reversal region (*a*). Cartoon of the edge of the Sun showing the inclination of the field projected on the sky. This is the basic principle of the Hale et al. technique for measuring inclination angle at the limb (*b*).

© American Astronomical Society • Provided by the NASA Astrophysics Data System

1993ApJ...403..780T

is 2β wide with boundaries at $\psi = \pi \pm \beta$. With these definitions the inclination angle of the field on the neutral line at the edge of the spot is given by

$$\gamma_{\text{reversal}} = \arctan\left(\frac{1}{\tan\theta\cos\beta}\right). \tag{7}$$

Hale et al. (1918) defined a sunspot neutral line as the line connecting the reversal points on the spot's outer boundary. The position of the neutral line was then used to infer the inclination of the magnetic field with respect to the surface. If the spot is assumed to be round and of unit radius, then cos (β) is just the distance from the center of the spot to the neutral line in the spot coordinate system.

$$\cos\beta = \left(\frac{1}{\tan\gamma_{\text{reversal}}\tan\theta}\right). \tag{8}$$

Unfortunately, β is not a very sensitive indicator of the inclination angle, γ. This makes it very difficult to determine from the displacement of the neutral line how much greater the inclination angle is than the complement of the heliocentric angle. This can be easily seen by defining an inclination enhancement factor, y, such that

$$\gamma_{\text{reversal}} = \pi/2 - \theta/y\,, \tag{9}$$

then

$$\beta = \arccos\,[\tan(\theta/y)/\tan\theta]\,. \tag{10}$$

Figure 3 shows plots of β versus y for heliocentric angles of 20° (*solid line*), 40° (*dashed line*), and 60° (*dot-dashed line*). For values of $y < 1$, there is no solution to equation (10) because there is no reversal of the line-of-sight field. As the heliocentric angle, θ, increases beyond the start of the reversal condition, the angle, β, over which reversal occurs increases very rapidly. Even for spots with relatively small heliocentric angles, it is difficult to establish enhancement factors much greater than 2. Thus, the neutral line method is of little value in precisely establishing the inclination of the field. However, reversal itself indicates that the inclination of the field is greater than the complement of the heliocentric angle. The closer the spot is to disk center the larger is the inclination angle that can be firmly established.

Hale et al. only reported on neutral line results for spots at heliocentric angles of 40° and greater, which from the above discussion are of limited value for determining inclinations near the boundary of the spot where the inclinations are often 70° or more. They must have recognized some of the difficulties raised in the above discussion because they only used their neutral line data for obtaining inclination angles up to the mid-penumbra. To measure the field inclinations in the outer penumbra, they measured the angle of the linear polarization in the Zeeman (π) component in the plane of the sky for spots just crossing the solar limb (see Fig. 2*b*). This method is elegant and very simple. However, it is affected by fields in the foreground and by telescope polarization, but neither of these problems are discussed in their papers.

Our magnetograms exhibit rapid variations in the line-of-sight component of the magnetic field in the penumbra which further complicates the standard neutral line approach. In order to gain insight into the sources of our observations we have constructed line-of-sight magnetogram patterns caused by simple perturbations on a cylindrical magnetic geometry. The pattern matching approach has the advantage of exhibiting characteristics of particular perturbation with azimuth around the spot and heliocentric location.

The line-of-sight component of the magnetic field of a cylindrically symmetric sunspot is from equation (1)

$$B_{\text{LOS}}(r_{\text{proj}}, \psi_{\text{proj}}, \gamma, \theta, \psi) = B(r)(\sin\gamma\sin\theta\cos\psi + \cos\gamma\cos\theta)\,. \tag{11}$$

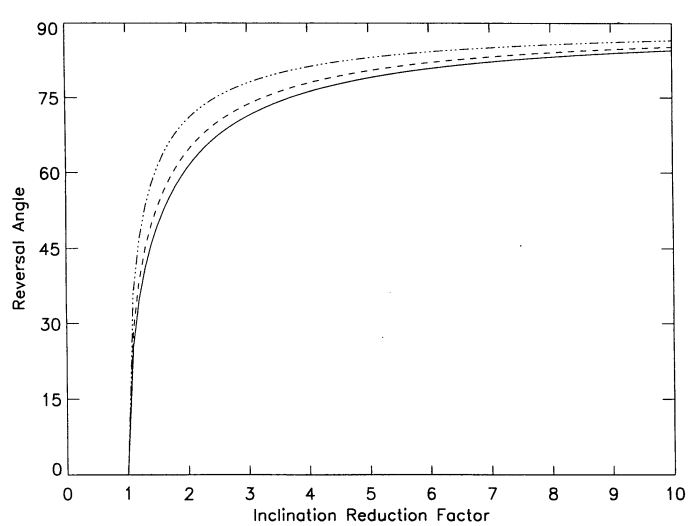

FIG. 3.—Plots of the opening angle of the neutral line, β, vs. the inclination modification factor, y, for heliocentric angles of 20° (*solid line*), 40° (*dashed line*), and 60° (*dash-dotted line*).

© American Astronomical Society • Provided by the NASA Astrophysics Data System

1993ApJ...403..780T

If the line-of-sight field is observed on an ellipse corresponding to a circle of constant radius in the spot, then the signal as function of ψ will be a single cycle of a cosine function with amplitude,

$$\text{Amp}\ (r) = B(r) \sin \gamma \sin \theta \tag{12}$$

with an offset of

$$\text{Mean}\ (r) = B(r) \cos \gamma \cos \theta\ , \tag{13}$$

due to the component in the spot z-axis direction.

If the signal changes in magnetograms were caused by an azimuthal variation in magnetic field strength, then $B(r)$ in equation (11) must be replaced by $[B(r) + \delta B(r, \psi)]$. Because the magnetogram signal is proportional to the angular dependent part of equation (11), when the angular dependent part of equation (11) is near zero, the entire magnetic signal including fluctuations will be near zero. Thus, a signature of rapid field strength variations alone is a lack of variations near the neutral line.

The observed magnetogram fluctuations do not go to zero in the vicinity of the neutral line. This means that there must be either variations in the azimuth and or elevation of the field perhaps coupled with fluctuations in the field strength. Therefore, we consider the effects of fluctuations in both the inclination and azimuthal angles. If the inclination angle variations are rapid with respect to azimuth around the spot, then to a good approximation the amplitude of the line-of-sight variations is given by

$$\text{Amp}\ B_\gamma(r_{\text{proj}}, \delta\gamma, \theta, \psi) = \tfrac{1}{2}[B_{\text{LOS}}(r_{\text{proj}}, \psi_{\text{proj}}, \gamma + \delta\gamma, \theta, \psi) - B_{\text{LOS}}(r_{\text{proj}}, \psi_{\text{proj}}, \gamma - \delta\gamma, \theta, \psi)]\ , \tag{14}$$

where $\delta\gamma$ is the amplitude of the fluctuation about the inclination, γ. Expanding equation (14) using equation (11) yields

$$\text{Amp}\ B_\gamma(r_{\text{proj}}, \delta\gamma, \theta, \psi) = -B(r) \sin (\delta\gamma)(\sin \gamma \cos \theta - \cos \gamma \sin \theta \cos \psi)\ , \tag{15}$$

which does not tend toward zero near the neutral line unless γ is close to θ, or for near vertical fields near disk center, a situation which does not occur in the penumbra. The amplitude of fluctuation is proportional to $-B(r) \sin (\delta\gamma)$ and is slowly modulated in azimuth around the spot by a projection factor which varies between $\sin (\gamma - \theta)$ and $\sin (\gamma + \theta)$. Near the outer penumbral boundary γ is near 70°. Hence, the projection factor is of significant amplitude at all azimuths when a spot is near disk center. This is in marked contrast to case where signal fluctuations are caused by rapid changes in field strength alone, for which the fluctuations go to zero in the vicinity of the neutral line.

If the magnetic field were twisted on the scale of the fibrils, then there would be rapid azimuthal change in the field direction. When the amplitude of the azimuthal fluctuation is $\delta\psi$, to a good approximation the amplitude of line of sight fluctuation is

$$\text{Amp}\ B_\psi(r_{\text{proj}}, \delta\psi, \gamma, \theta, \psi) = -B(r) \sin (\delta\psi) \sin \gamma \cos \theta \sin \psi\ , \tag{16}$$

where $\delta\psi$ is the amplitude of the rapid fluctuation in the azimuth angle. Here the line of sight fluctuation is zero in the Sun center and limb directions and is maximal along the y axis. So like the magnetogram signals caused by fluctuations in field strength, there are broad ranges in azimuthal where the fluctuations go toward zero.

Equations (11) through (16) indicate the forms of the line-of-sight magnetic field variations expected around the spot from fluctuations in magnetic field strength, inclination angle, and azimuth angle. To generate insight into the appearance of spots we follow the path of Maltby (1964) and generate magnetogram signal patterns modified by rapid sine wave fluctuations due entirely to either field strength, inclination, or azimuth variations. For the field strength fluctuations, we take

$$\frac{\delta B(\psi)}{B_0} = 0.2 \sin (30\psi)\ , \tag{17a}$$

for the inclination fluctuations

$$\delta\gamma(\psi) = -15 \sin (30\psi)\ , \tag{17b}$$

and for the azimuthal variations

$$\delta\psi(\psi) = -20 \sin (30\psi)\ . \tag{17c}$$

The maximum signal has been set to unity in all cases. The ordinates of the graphs in Figures 4 and 5 are, therefore, labeled relative signal.

We have chosen 30 cycles of fluctuations around the spot for the convenience of the display. Figure 4 shows the relative line of sight and transverse magnetic signals caused by fluctuations in field strength (*top*), inclination (*middle*), and azimuth (*bottom*) and without fluctuations for the case where γ and θ are 70° and 20°, while Figure 5 shows similar plots the case where γ again equals 70°, but where the heliocentric angle, θ, is increased to 40°. In both figures the dashed plots are those for the cylindrically symmetric line of sight fields and the dash dotted plots are for the cylindrically symmetric transverse fields.

It should be clear from Figures 4 and 5 that the line-of-sight and transverse magnetogram signals spot have different characteristic patterns depending on whether they are caused by fluctuations in field strength, inclination, or azimuth. Fluctuations of the line-of-sight magnetic signals are large all around the spot only in the case where the inclination angle varies. Line-of-sight signals caused by fluctuations in either field strength or azimuth go relatively slowly toward zero over some distance around the spot. For the transverse magnetic signals only those modified by the variations in field strength are large all around the spot, while signal fluctuations caused by inclination and azimuth variations both disappear over ranges in angle. Even if real spots are not perfectly symmetric, the overall forms of the longitudinal and transverse magnetogram signals caused by fluctuations in field strength, inclination and azimuth persist.

© American Astronomical Society • Provided by the NASA Astrophysics Data System

1993ApJ...403..780T

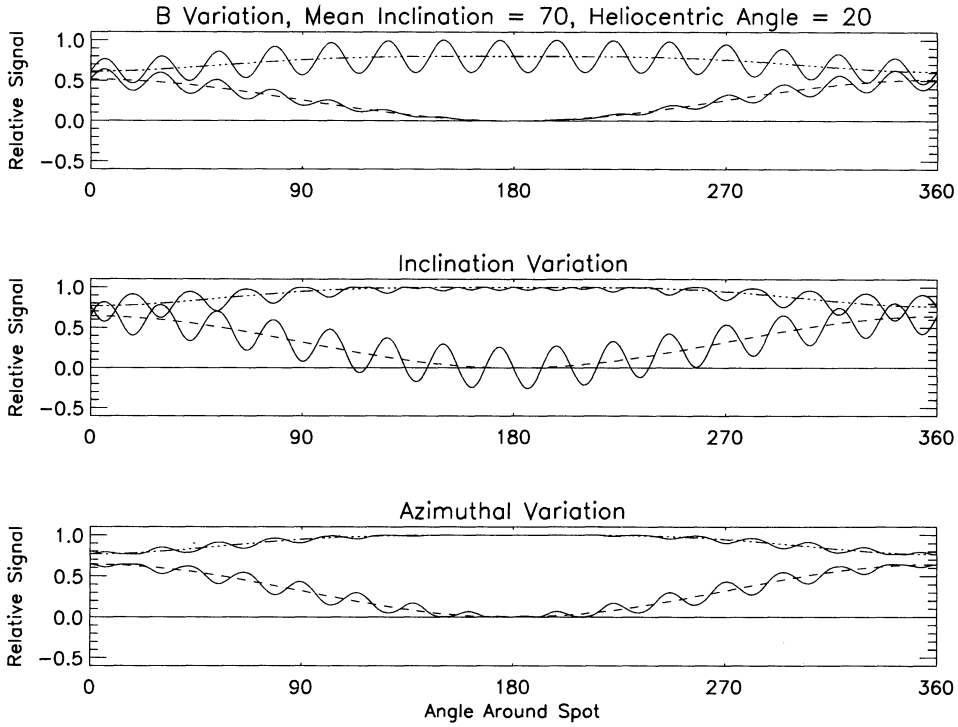

FIG. 4.—Plots of the relative line-of-sight and transverse magnetogram signals for a cylindrically symmetric spot and a spot with azimuthal perturbations for the cases where the variations are caused by fluctuations in the magnetic field strength (*top*), the inclination of the field (*center*), and the azimuth of the field (*bottom*) for a mean inclination angle of 70° and a heliocentric angle of 20°. The cylindrically symmetric line-of-sight and transverse results are shown as the dashed and dash-dotted lines, respectively.

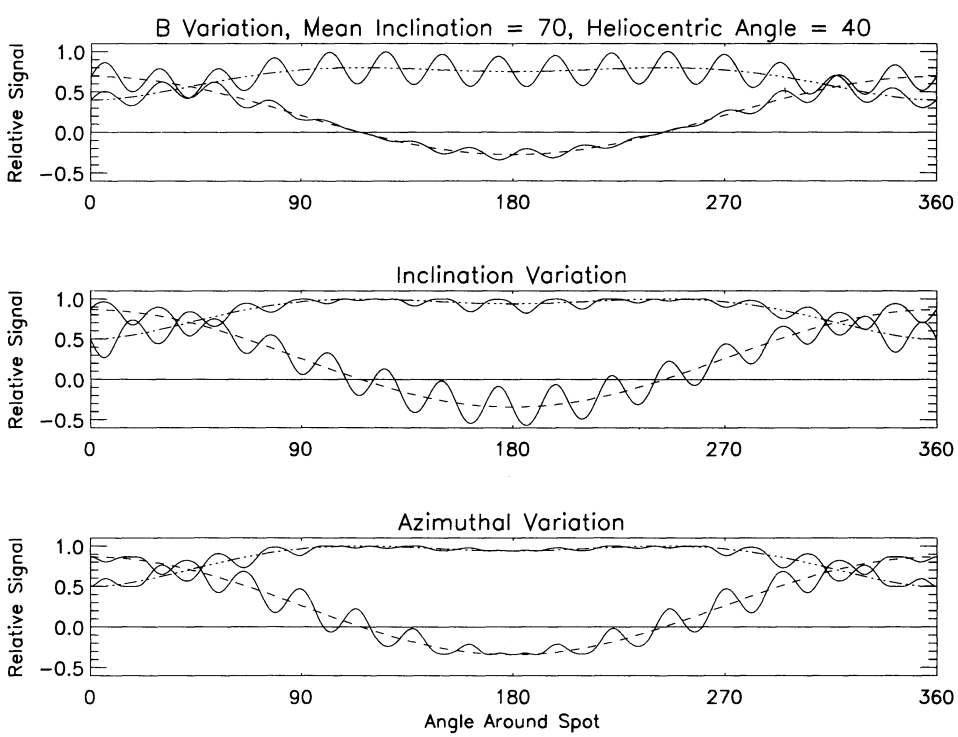

FIG. 5.—Same format as Fig. 4, but for a heliocentric angle of 40°

© American Astronomical Society • Provided by the NASA Astrophysics Data System

1993ApJ...403..780T

4. DATA ANALYSIS

4.1. *Traversal of a Simple Round Spot*

Figure 6 (Plate 1) shows magnetograms of our simple round spot in AR 5168 on September 14 ($\theta = 40\overset{\circ}{.}2$), 16 ($\theta = 20\overset{\circ}{.}1$), 17 ($\theta = 18\overset{\circ}{.}6$), and 20 ($\theta = 41\overset{\circ}{.}8$) 1988. The arrows on the figure indicate the direction of the center of the Sun. White (black) regions are locations where the line-of-sight field is positive (negative). The Sun center side of the spots is always white. The reversals of the line of sight field due to projection effects are clearly visible as black areas on all of the days. The existence of black areas in the magnetograms on the September 16 and 17 reveal the presence of field inclinations greater than 70°. But note that the reversal areas also contain thin white lines which indicate locales where the inclinations are less than 70°.

For this analysis, we assumed that the spot was circular. Unfortunately, as with any real spot there will always be some imperfections of the circularity of both the umbra and penumbra, so that the first problem was to decide on the location of the center of the spot with respect to the penumbra. To do this, an image of the spot in the continuum was displayed and an ellipse (to account for the projection of the spot onto the observation plane) was drawn on the spot approximately centered in the penumbra. Since the continuum intensity on a constant radius in a simple round spot should not be dependent on angular position around the spot, the intensity along the perfectly placed ellipse should fluctuate only because of the presence of fibril structure in the penumbra. In a real sunspot there will also be an intensity variation due to the deviation from perfect symmetry. To determine the quality of the center estimate, the continuum intensity along the ellipse was Fourier transformed. (The zeroth Fourier amplitude is the mean along the ellipse.) If the ellipse is well centered, then the first few Fourier amplitudes should be smaller than those of other ellipses of the same size but displaced. To validate centering Fourier amplitudes were calculated for an array of locations around the initial guess of the center. Only the center was varied. The orientation and size of the ellipse remained constant.

Spot centers were determined using the above procedure for a series of ellipses which go from just inside the umbral boundary to well outside the penumbral boundary. For each case, the best ellipse path had low-order variations of 1% to 5% of the mean intensity. But paths near the chosen fits were not much worse. The spot center was determined from the mean of the centers of the ellipses well contained in the penumbra, i.e., those with semi-major axes from 70 to 100 pixels (11″.62 to 16″.6). Shown in Figure 7 (Plate 2) (*top*) is a September 17 continuum image overlayed by ellipse paths. For clarity only a subset of the paths are shown. The complete set of paths span semi-major axes from 40 to 180 pixels (6″.48 to 29″.16) with 10 pixel (1″.62) spacing or from well inside the umbra to well outside the penumbra.

Once the set of ellipse paths was determined it was simple to obtain the line-of-sight magnetic field along the spot radii because the magnetogram and continuum images were aligned to better than 0″.1. Figure 7 (*bottom*) shows the ellipse paths on the corresponding magnetogram. The best fit to the mean signal and single cosine cycle was calculated from each of the magnetogram traces. In fitting the cosine to the trace we allowed the phase to vary to allow for slight global twists of the field. The power spectrum along each path was calculated and the noise level of the magnetic signal estimated. The noise level and the zeroth (mean) and first Fourier components were subtracted from the Fourier expansion and the series was inverse transformed. The resulting signals are then only due to local variations in the line-of-sight magnetic field. As an example of the process, the magnetogram signal overlayed with the best-fit offset cosine function and the magnetogram signal with the mean, cosine modulation, and noise removed versus azimuth angle are shown in Figure 8*a* and 8*b*, respectively, for an ellipse path in the mid-penumbra on September 17 data.

By inspection of Figure 8 and the arguments above, it was clear that most of the observed fluctuations were caused by rapid inclination changes. This discrimination is largely based on the nearly constant amplitude of the fluctuations around the spot. If the

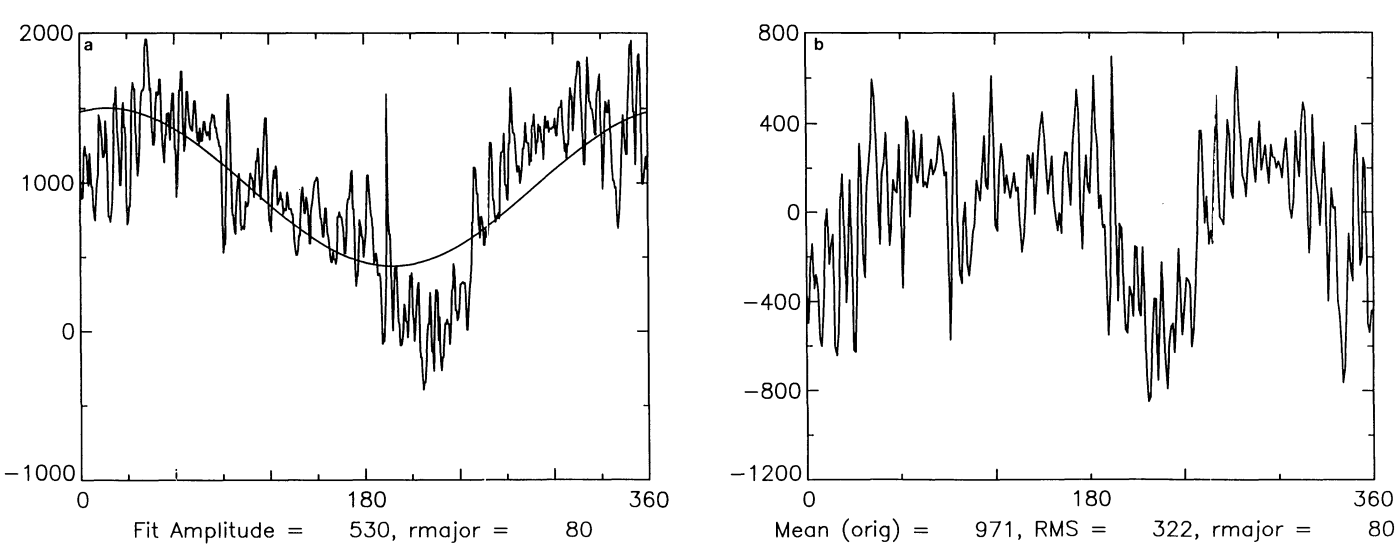

FIG. 8.—Magnetic field signal on an ellipse through the mid-penumbra of the 1991 September 17 15:57 UT magnetogram (*a*) and the same signal with the first Fourier component, mean, and white noise removed (*b*) vs. angle around the stop. The solid line is the best fit of an offset cosine function. Zero degrees is in the direction towards disk center. Tick marks are at 60° intervals which corresponds to 13″.9 along the circumference of the spot.

© American Astronomical Society • Provided by the NASA Astrophysics Data System

1993ApJ...403..780T

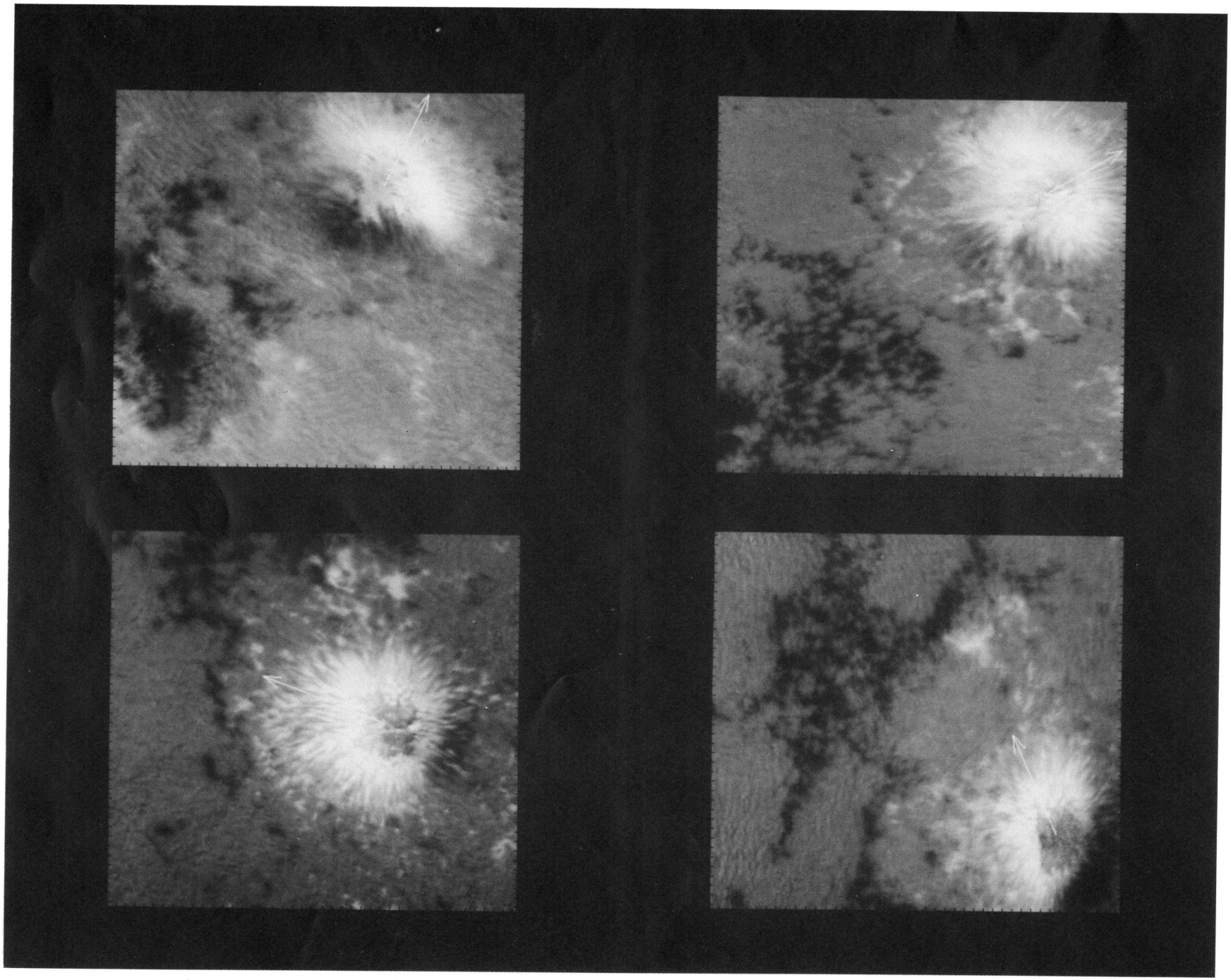

FIG. 6.—From upper left to lower right line-of-sight magnetic field maps (magnetograms) of the simple round spot in AR 5168 on 1988 September 14, 16, 17, and 20. On these days the heliocentric positions of spot center were 40°.2, 20°.1, 18°.6, and 41°.8, respectively. The arrow on each map indicates the direction toward the center of the Sun. The field of view of each image is 82″ and the interval between ticks is 2″.

TITLE et al. (see 403, 787)

© American Astronomical Society • Provided by the NASA Astrophysics Data System

1993ApJ...403..780T

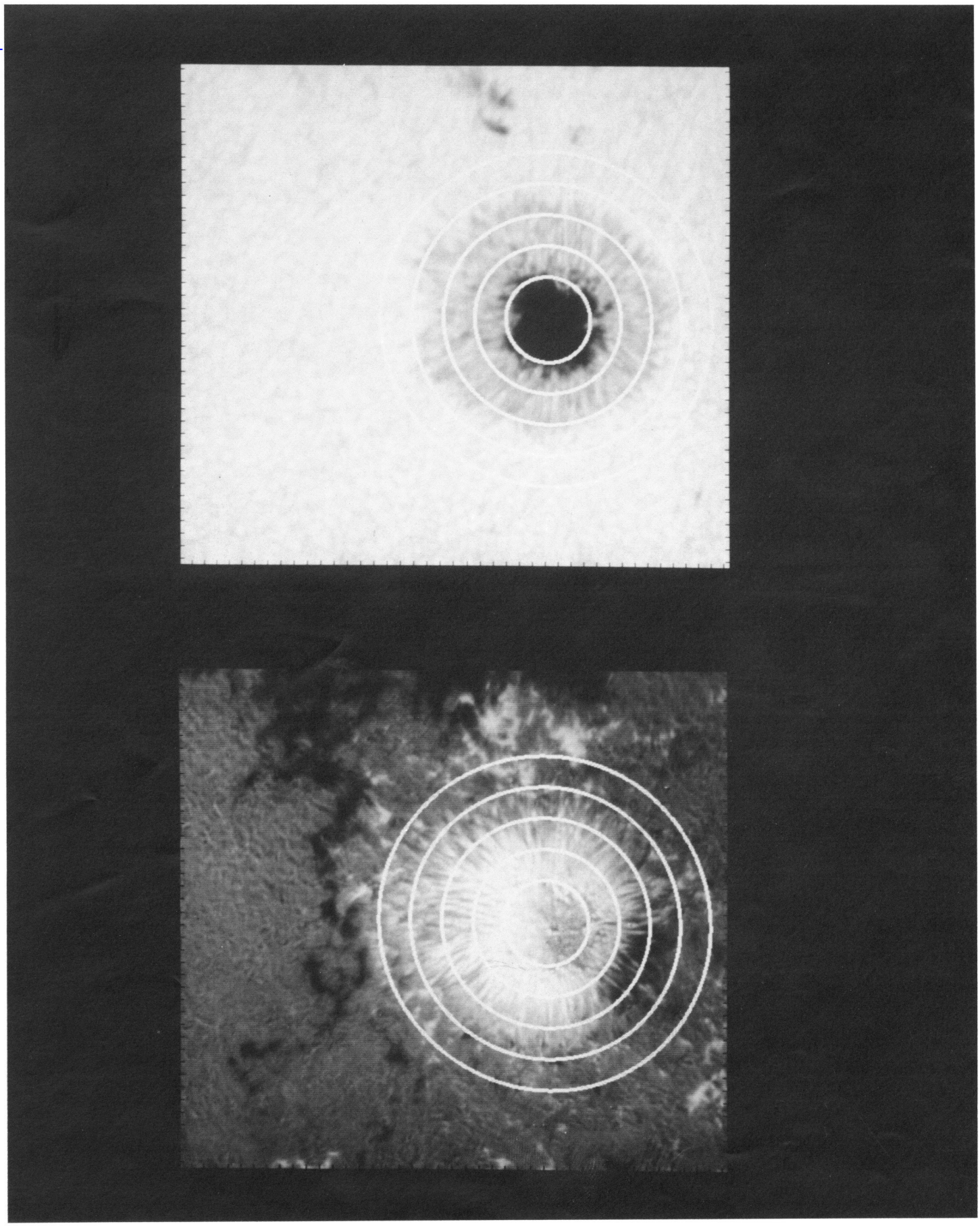

FIG. 7.—Constant radii paths in the observation plane shown on the continuum (*top*) and line-of-sight magnetic field (*bottom*) maps of one of the September 17 15:57 UT data. On the magnetic field map, the field strength is saturated at 1000 G in the photospheric image.

© American Astronomical Society • Provided by the NASA Astrophysics Data System

1993ApJ...403..780T

fluctuations were due only to either a variation in field strength or rapid changes in azimuth angle the fluctuations would have dropped to zero over a range in azimuth. We cannot rule out the presence of small fluctuations in magnetic field strength or small azimuthal twists, but for this analysis we assume that the magnetic field strength is only a function of radius.

By measuring the amplitude (eq. [12]) and mean (eq. [13]) of a trace at a particular spot radius, r, the average inclination angle, $\gamma_{\rm mean}(r)$, is determined (the heliocentric angle, θ, is known), so that

$$\gamma_{\rm mean}(r) = \text{arcctn}\left[\frac{\text{Mean }(r)}{\text{Amp }(r)}\tan\theta\right]. \tag{18}$$

Because equation (18) is a ratio of magnetogram signals at the same radius, the direct dependence of on field strength disappears. Thus, this result is relatively insensitive to calibration of the magnetogram signal. However, the calibration is still affected by changes in the profile along the trace.

The magnetic field strength estimate follows from the above result and equation (13), so that

$$B(r) = \frac{\text{Mean }(r)}{\cos\gamma_{\rm mean}(r)\cos\theta}. \tag{19}$$

Since the mean value of the line-of-sight magnetic field is subject to the errors in the calibration of our magnetogram signal, the field strength is subject to an uncertainty of about 40%. Also because cos ($\gamma_{\rm mean}$) is lowest at the outer penumbral boundary the field strength is most uncertain there. An uncertainty of 5° in the inclination at the boundary causes a 30% change in the field strength. Therefore, the field strength estimates are not very useful for distinguishing sunspot models.

If all the magnetogram fluctuations occur because of inclination variations, then the amplitude of the magnetogram signal variation caused by an inclination fluctuation of $\pm\delta\gamma$ is determined by the ratio of the rms fluctuation in the magnetogram signal to the mean field strength through

$$\sin[\delta\gamma(r)] = \frac{B_{\rm rms}\sqrt{2}}{B(r)}\left(\sin^2\gamma\cos^2\theta + \frac{1}{2}\cos^2\gamma\sin^2\theta\right)^{-1/2}. \tag{20}$$

Like the inclination measurement, the amplitude of the inclination variation is a ratio of magnetogram signals and is relatively free of our calibration of the magnetogram signal.

The mean inclination angle, $\gamma_{\rm mean}(r)$, its variation, $\delta\gamma(r)$, and $B(r)$ were calculated for line of sight magnetograms taken at 8:45 UT and 9:16 UT on September 16 and 15:45 and 15:57 UT on September 17. For each of the data sets a set of ellipse paths of widths 1 and 5 pixels (0".162 and 0".81) was used. The results are shown in Figure 9 for the single pixel wide data. The data for the 5 pixel average are virtually identical. The two data sets taken on the 16th are shown as "stars" and "pluses" while those taken on September 17 are shown as open "diamonds" and "squares". Solid lines connect the mean of the four measurements at radial positions from 40 to 120 pixels. In both figures the normalized mean and the rms continuum intensity are shown in the lower right panel. All of the functions are plotted as a function of spot radius in pixels.

From the lower right panel it can be seen that umbra-penumbra and outer penumbral boundaries are at about 60 and 120 pixels (9".7 and 19".5), respectively. The normalized mean intensity rises gradually between 100 and 135 pixels because the sunspot boundary does not have the same radius at all azimuths. Because the lack of ellipticity of the outer boundary and its roughness the rms intensity variation shows a broad peak in the region where the continuum intensity is rising. The sharp rise in the rms intensity at the umbra-penumbra boundary is caused for similar reasons.

Two adjacent cycles of data on each day were reduced to estimate the effect of misregistration on the results. From the figure it is clear that the results obtained from the close data pairs are very similar. Because the spot traverses the central meridian between the observations of September 16 and 17, the reversal regions are on opposite sides of the spot on these two days. The close agreement of the results from observations on these two days suggests that lack of symmetry in the spot also has little effect on the results.

The single and 5 pixel wide data have similar spatial resolution because the penumbral structures are primarily radial. Therefore, the component of the rms magnetogram variation caused by inclination variation should only be slightly reduced. However, the noise component of the 5 pixel wide data should be factor of 2.2 lower than for the single trace data. The close agreement between the inclination variation estimates obtained from the two data sets strongly indicates that noise is a minor factor.

Direct estimates of the noise in the magnetograms were made by subtracting registered and destretched filtergrams made in the *same* circular polarization taken in the wing of Fe 6302 Å. The magnetogram signal in these calibration tests have a misregistration signal of about 50 G, which is considerably smaller that the 400 G fluctuations observed in the mid-penumbra.

Errors in the location of the center and/or noncircular penumbra can cause an error in both the amplitude and the mean of our circular traces. However, the centering experiments indicate the centering error is much less than the 10 pixel spacing of the ellipses. The error in mean inclination is less than a degree from this source.

We have measured the polarization of the La Palma telescope using a full aperture polarizer and quarterwave plate and have determined the Mueller matrix of the telescope for several orientations of the mirrors. We are confident that the line-of-sight measurements are not much affected by telescope polarization. The Mueller matrix of the telescope allows a very small loss of the V-signal, but indicates there is some conversion of linear polarized light in certain orientations into the circular. Because of potential for a problem, we have here reported on measurements made at approximately 6 hr apart in time of day. With this time difference the relative positions of the azimuth and elevation mirrors change considerably and therefore the coupling of linear to circular polarization also differs considerably. Further, because the magnetic field in the spot is basically radial, a linear polarization

© American Astronomical Society • Provided by the NASA Astrophysics Data System

1993ApJ...403..780T

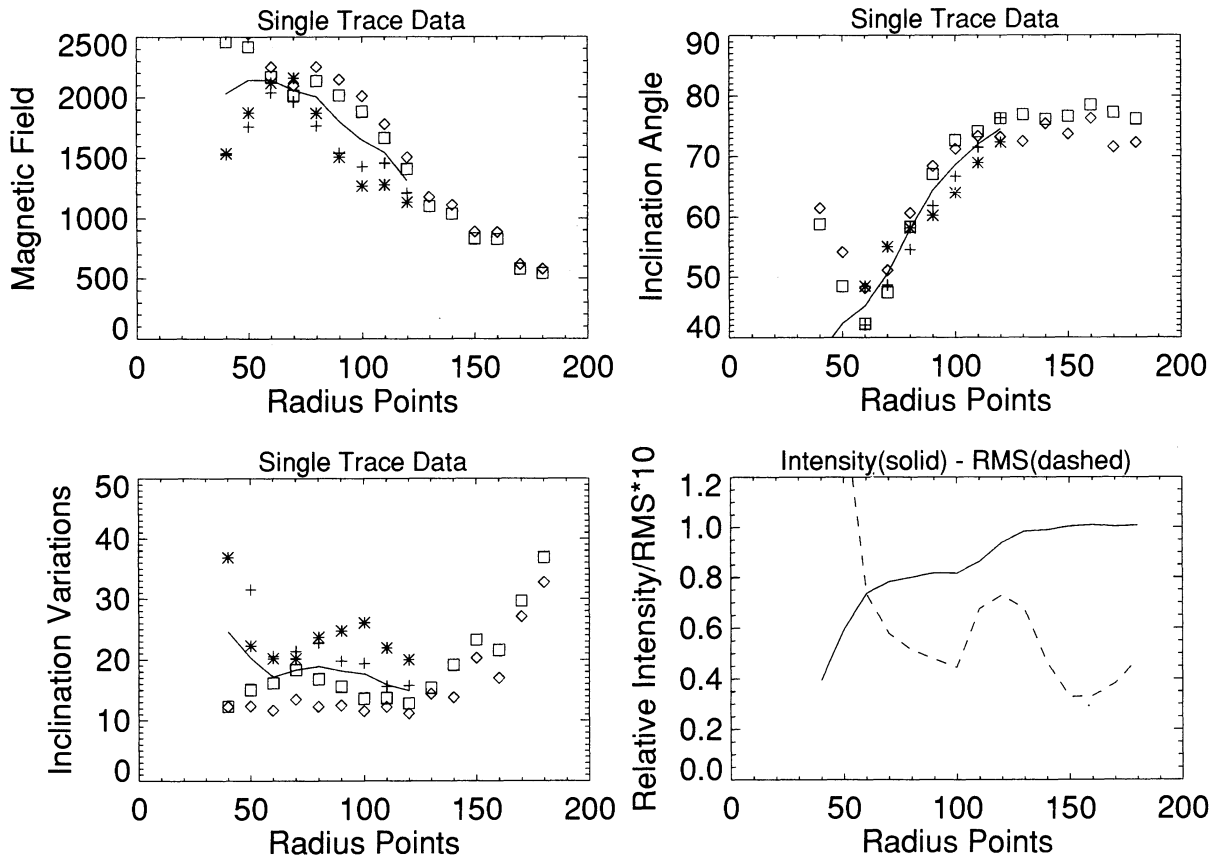

FIG. 9.—Plots from upper left to lower right of magnetic field strength, inclination angle, and amplitude of the inclination fluctuation vs. spot radius in pixels. The stars and pluses and the open diamonds and squares indicate the results for the two data sets taken on September 16 and 17, respectively, for the single pixel wide data. The solid lines connect the mean value at each radius. The lower right panel shows the normalized (*solid line*) and rms (*dashed line*) continuum intensity times 10 vs. radius for a September 17 data set.

coupling would cause an oscillation in the V signal that varies like $\cos^2(\psi)$. Therefore, it causes almost no effect on our estimate of the amplitude and has only a relatively small effect on the mean signal. A 20% coupling of linear circular polarization would cause about a 2° error in the mean inclination angle for radii in the penumbra. The close agreement of the data taken on September 16 and 17 substantiates that telescope polarization does not have a large effect on the measurements.

The inclination and inclination variation results are both the most interesting and most reliable results of this analysis. We find a steady drop in mean inclination angle of the magnetic field across the penumbra, with value of about 72° at the boundary with the photosphere. These data also exhibit a 30% to 40% variation in the line-of-sight magnetic signal on scale of the penumbral fibrils. This can be explained with a mean amplitude of the fluctuation in the inclination angle of $\pm 18°$. Taken together with the mean inclination at the outer penumbral boundary, our results indicate that the magnetic field vector at the outer penumbral boundary is varying between 54° and 90° on the spatial scale of the penumbral fibrils.

4.2. *Line-of-Sight "Spectral" Data for a Spot*

The data taken of a relatively simple spot in AR 6122 on 1990 June 28 ($\theta = 28\overset{\circ}{.}6$) allowed the construction of line-of-sight velocity and line-of-sight magnetic maps, continuum images, and "spectra" with a resolution of about 88,000. An interactive video display program developed by one of us (R. A. S.) allowed display of any the filtergrams, magnetograms, or Dopplergrams in a data set, where here a data set is a complete spectral sequence. Figures 10*a*–10*d* (Plates 3–6) shows a Fourier Dopplergram, a magnetogram made at -60 mÅ from line core, a magnetogram in line core, and a continuum image. In the figure white (black) indicates the true (projection reversed) polarity and an outward (inward) flow in the Dopplergram. The figure clearly shows that the flow pattern is more horizontal than the magnetic field. The Dopplergram signal is reversed virtually everywhere on the limb side of the spot, whereas the magnetogram exhibits the true polarity in the inner penumbra and in fine strips that extend to the outer penumbral boundary on the limb side. Also the figure shows that the Evershed flow drops abruptly at the outer penumbral boundary, while the magnetic field extends well beyond the boundary.

Spectra were created by choosing an image and then drawing a path on that image with the display cursor (a mouse). The software extracted the data from corresponding points on all the images, so that a synthetic slit of any shape and orientation could be placed on the spot structure. The slit is 1 pixel wide (0″.16). We have explored a large array of paths. These have included simple tangential and radial slits and more complex paths which followed features such as bright and dark fibrils seen in the continuum and

© American Astronomical Society • Provided by the NASA Astrophysics Data System

1993ApJ...403..780T

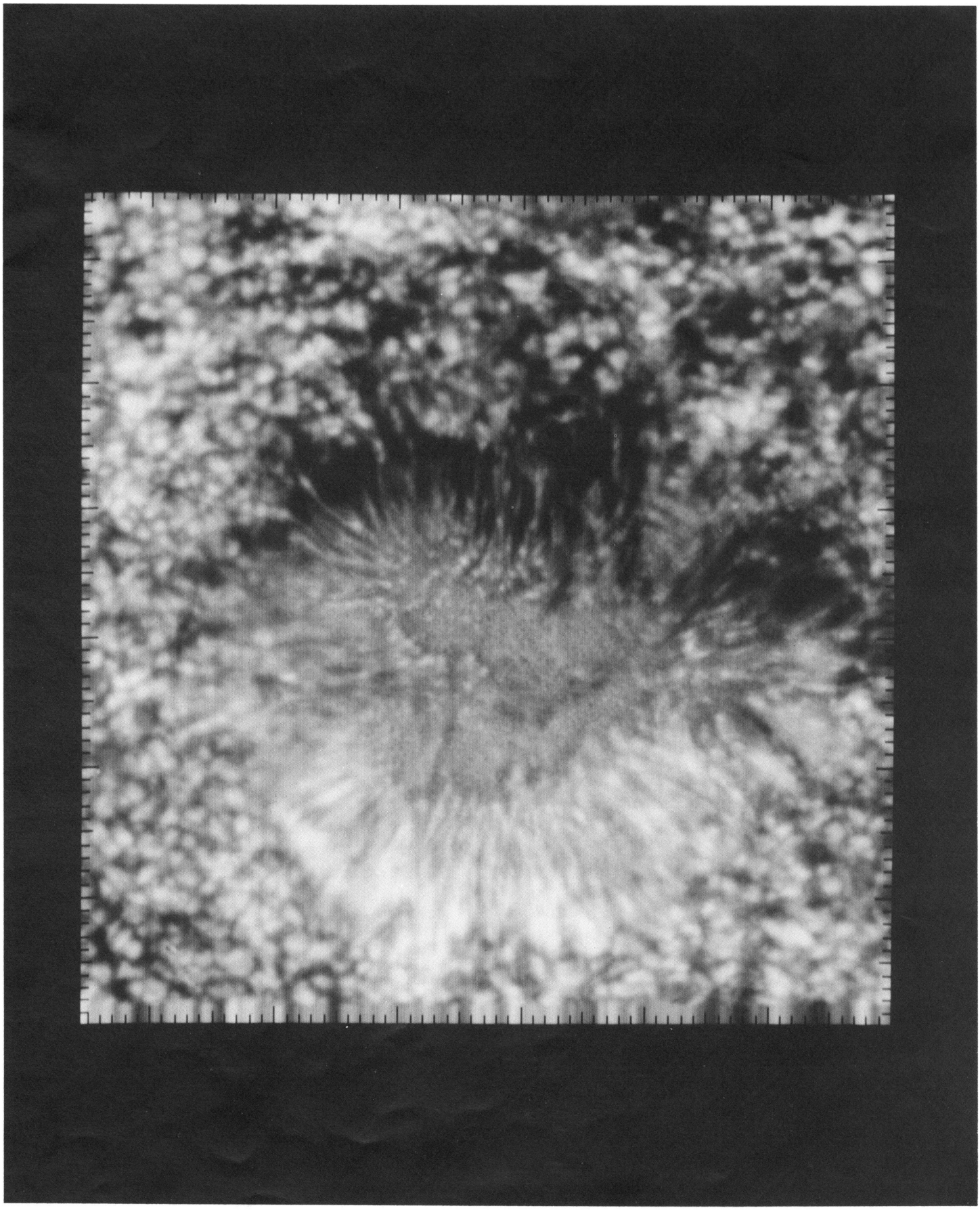

FIG. 10*a*

FIG. 10.—Fourier Dopplergram, −60 mÅ magnetogram, line center magnetogram, and continuum image for the 1990 June 28 data ($\theta = 24°.6$). White (black) indicates magnetic polarity. Solar north is at the top of the image. Pixel sizes are 0.6 and 0.8 arcsec in the horizontal and vertical directions, respectively.

©American Astronomical Society • Provided by the NASA Astrophysics Data System

1993ApJ...403..780T

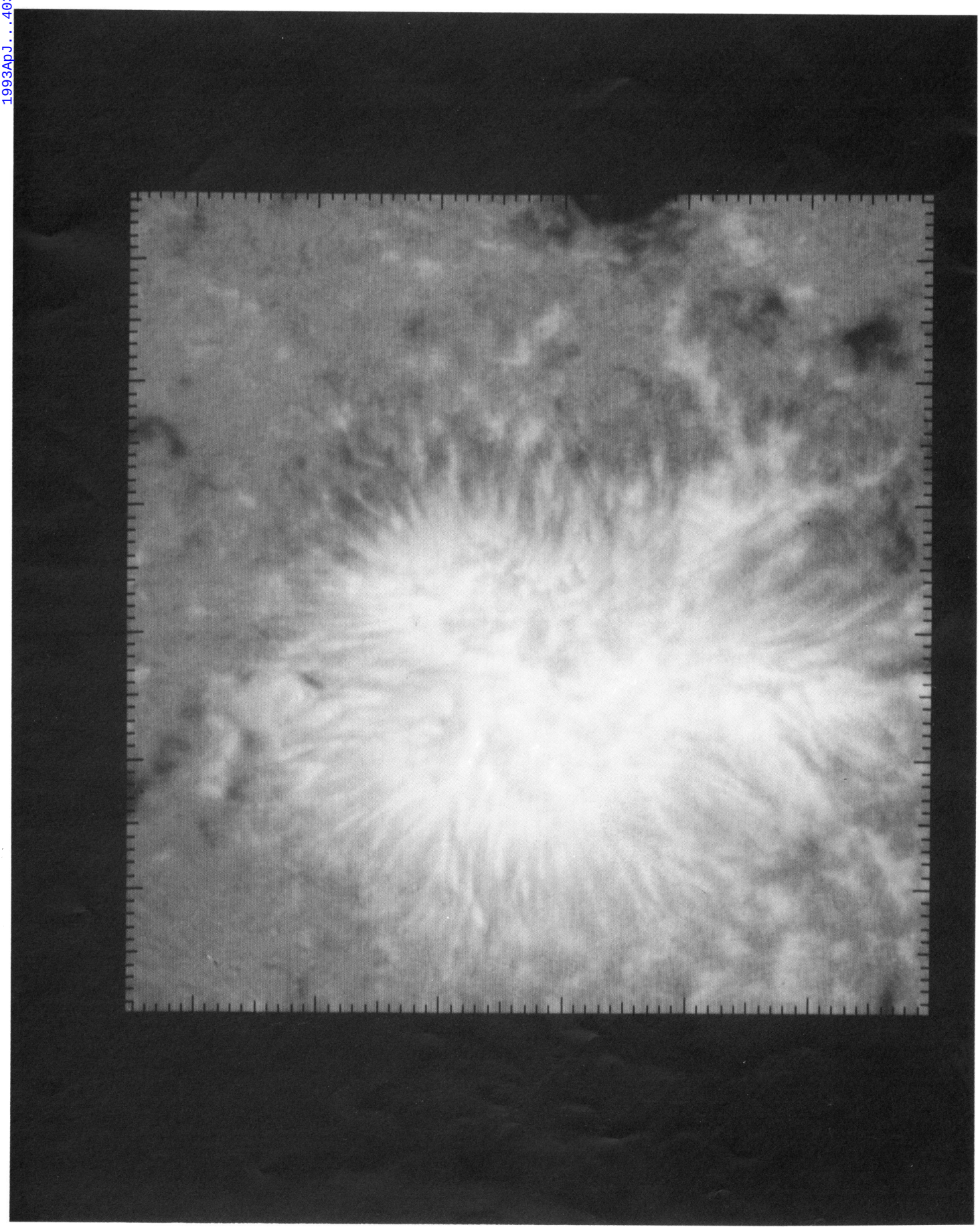

FIG. 10*b*

© American Astronomical Society • Provided by the NASA Astrophysics Data System

1993ApJ...403..780T

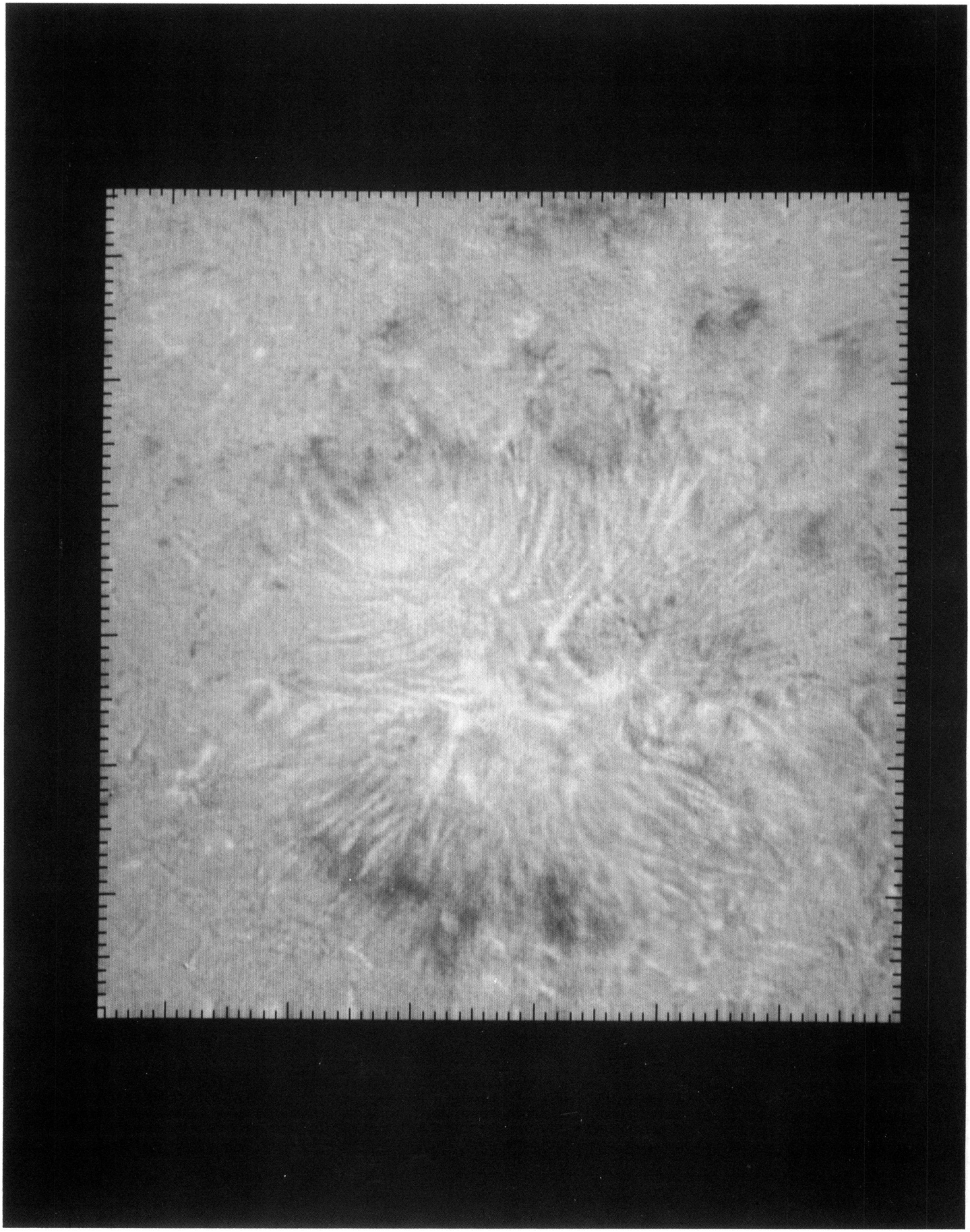

FIG. 10c

© American Astronomical Society • Provided by the NASA Astrophysics Data System

1993ApJ...403..780T

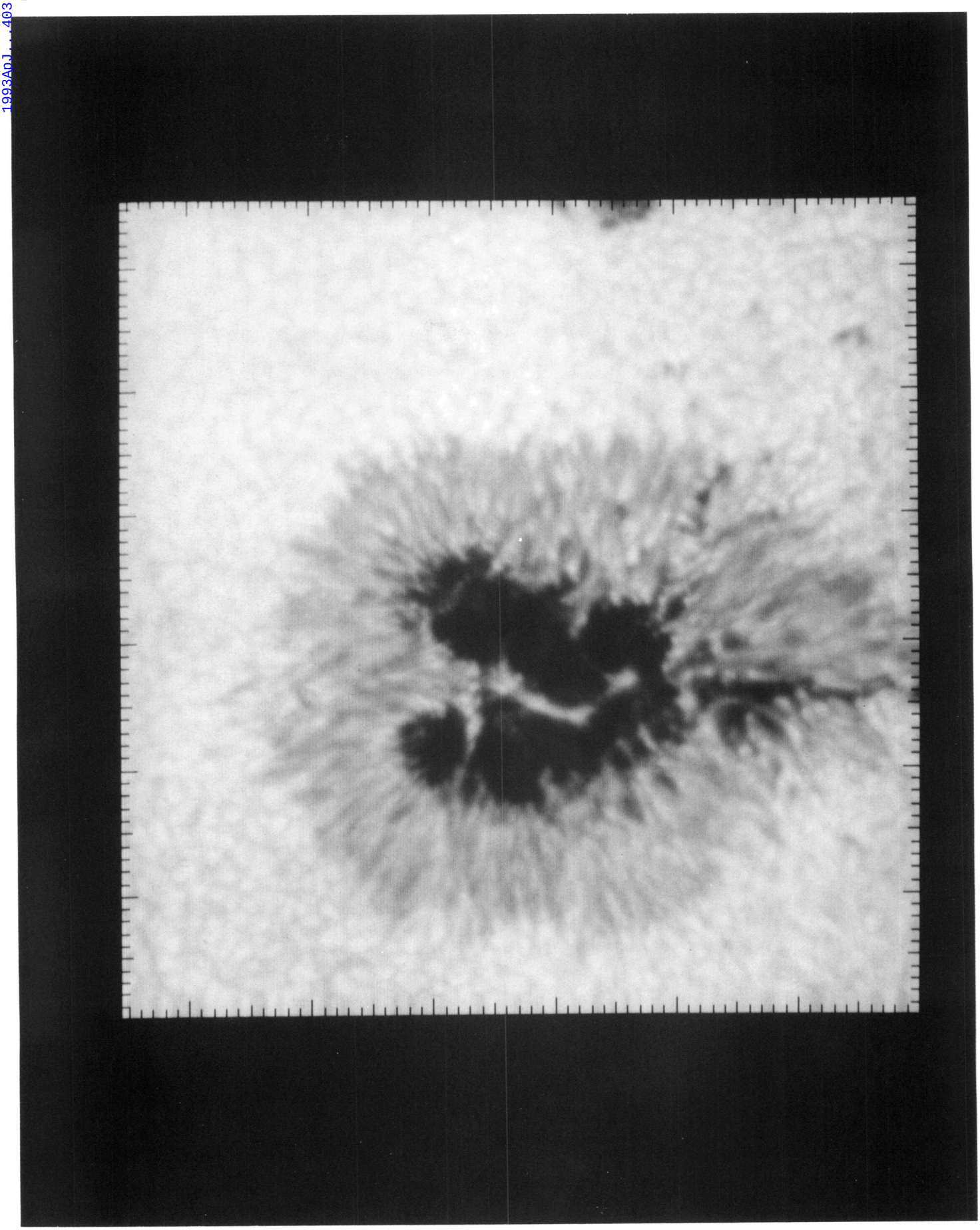

FIG. 10*d*

© American Astronomical Society • Provided by the NASA Astrophysics Data System

1993ApJ...403..780T

spectal images. An example of the slit extraction process is shown in Figure 11 (Plate 7) which contains a continuum image overlayed by 11 paths. Lines 1 through 5 are on the limb side of the spot at increasing distances from the outer penumbral boundary, and lines 6 through 11 are a similar set of paths on the disk center side of the spot. Also shown on the figure are the Fourier Doppler signals, the synthesized line profiles in Fe 5576 Å, the V-profiles (the difference between the right and left circular polarization profiles), and the right and left circular polarization profiles in Fe 6302 Å along slices 2 (limb) and 7 (center). In each of the profiles space is in the horizontal direction and wavelength is in the vertical direction. Note that the V-profiles on the disk center side, line 7, show no reversals, while the V-profiles on the limb side, line 2 show numerous reversals.

The top panels of Figures 12 and 14 shows the -30 mÅ magnetogram signal, the Dopplergram signal, and the continuum intensity along paths 2 and 7, respectively. The bottom panel of the figures show the same data with a third-order fit removed. Figures 13 and 15 display scatter plots and correlation coefficients for the magnetogram and Dopplergram traces in the upper left, the same data with the trends removed are shown from upper right to lower right and for the magnetogram and continuum, and the Dopplergram and continuum data. Also shown on the figure are the mean values of the magnetogram, Dopplergram, and continuum signals. Tables 1 and 2 lists these correlations and mean values for all paths for magnetograms made at -30 and -60 mÅ from the line core, respectively.

The mean values of the Doppler velocity are negative for all the limb paths. These data are consistent with an inclination of the flow field of greater than 65°.4 everywhere in the penumbra and greater than 84° in the outer penumbra. The data indicate that the Evershed flow has a range in speed with a maximum of nearly 4 km s^{-1}. The mean magnetic data indicates that the magnetic field is usually inclined at greater than 65° on paths 1 through 3.

On all the disk center paths the correlation coefficient between the magnetogram and Dopplergram signals are negative, which indicates that when magnetogram signal increases the Dopplergram signal tends to decrease. From the results above and those of Lites et al., at a constant radius (on a single path) the magnetic field strength is nearly constant and the magnetogram fluctuations are due to inclination changes in the magnetic field vector. Increasing magnetogram signal occurs with more vertical fields. The Evershed flow is nearly horizontal, so that the negative correlation coefficients indicate the flow speeds increase (decrease) where the magnetic fields are more horizontal (vertical). On the limb paths the correlation coefficients between the magnetogram and Doppler signals are positive which indicates that the signals tend to increase and decrease together. Magnetic fields that have greater than 65°.4 inclination to the local vertical on the limb paths have a negative projection along the line of sight. When the field becomes more parallel to the surface its projection along the line of sight increases in magnitude. The flow fields being nearly parallel to the surface have a negative projections along the line of sight, so that a positive correlation coefficient between the magnetogram and Dopplergram signals also indicates that horizontal magnetic fields are correlated with high outflow speeds. The correlation of velocity and magnetic field impacts our earlier estimate of the mean inclination angle; however, the effect is much less than 1° and we can neglect it.

The correlation between horizontal magnetic fields and horizontal flow patterns explains an initially confusing observation. The line center magnetogram, Figure 10c, shows a relatively strong negative (reversed polarity) signal just inside the outer penumbral

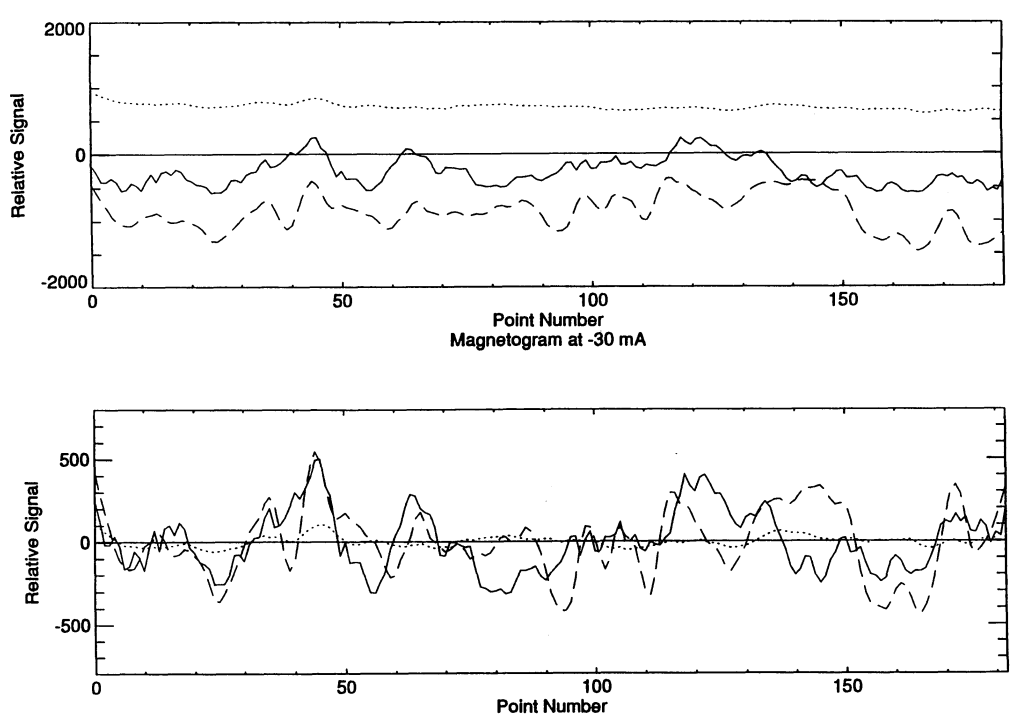

FIG. 12.—Upper panel contains plots of the line of sight magnetic field at -30 mÅ from line center Fe 6302 Å (*solid line*), the Fourier Doppler velocity (*dashed line*), and the continuum intensity (*dotted line*) for path 2, which is on the limb side of spot. The lower panel shows the same curves with a third-order fit to the data removed.

© American Astronomical Society • Provided by the NASA Astrophysics Data System

1993ApJ...403..780T

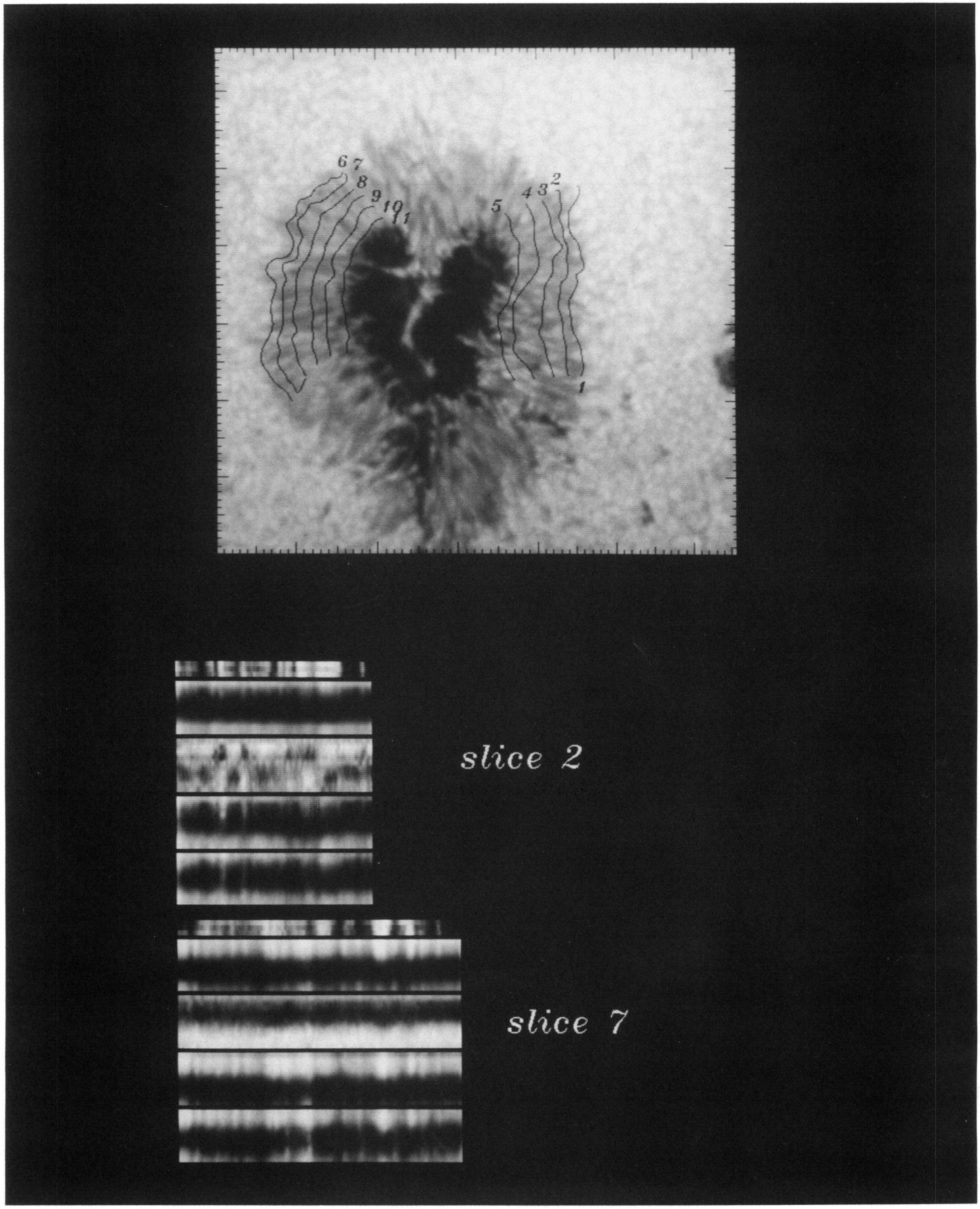

FIG. 11.—Continuum image of the June 28 spot overlayed with the paths used for creating spectra. Paths 1–5 and 6–11 are on the limb and center side of the spots, respectively. Also shown on the figure are arrays of spectra from paths 2 and 7. Each array consists of the Fourier Doppler velocity, spectra in Fe 5576 Å, the V-profile and profiles in right and left circular polarization in Fe 6302 Å. In all the profiles distance along the Sun is in the horizontal direction and wavelength is in the vertical direction. The scale is 1 arcsec per pixel.

© American Astronomical Society • Provided by the NASA Astrophysics Data System

1993ApJ...403..780T

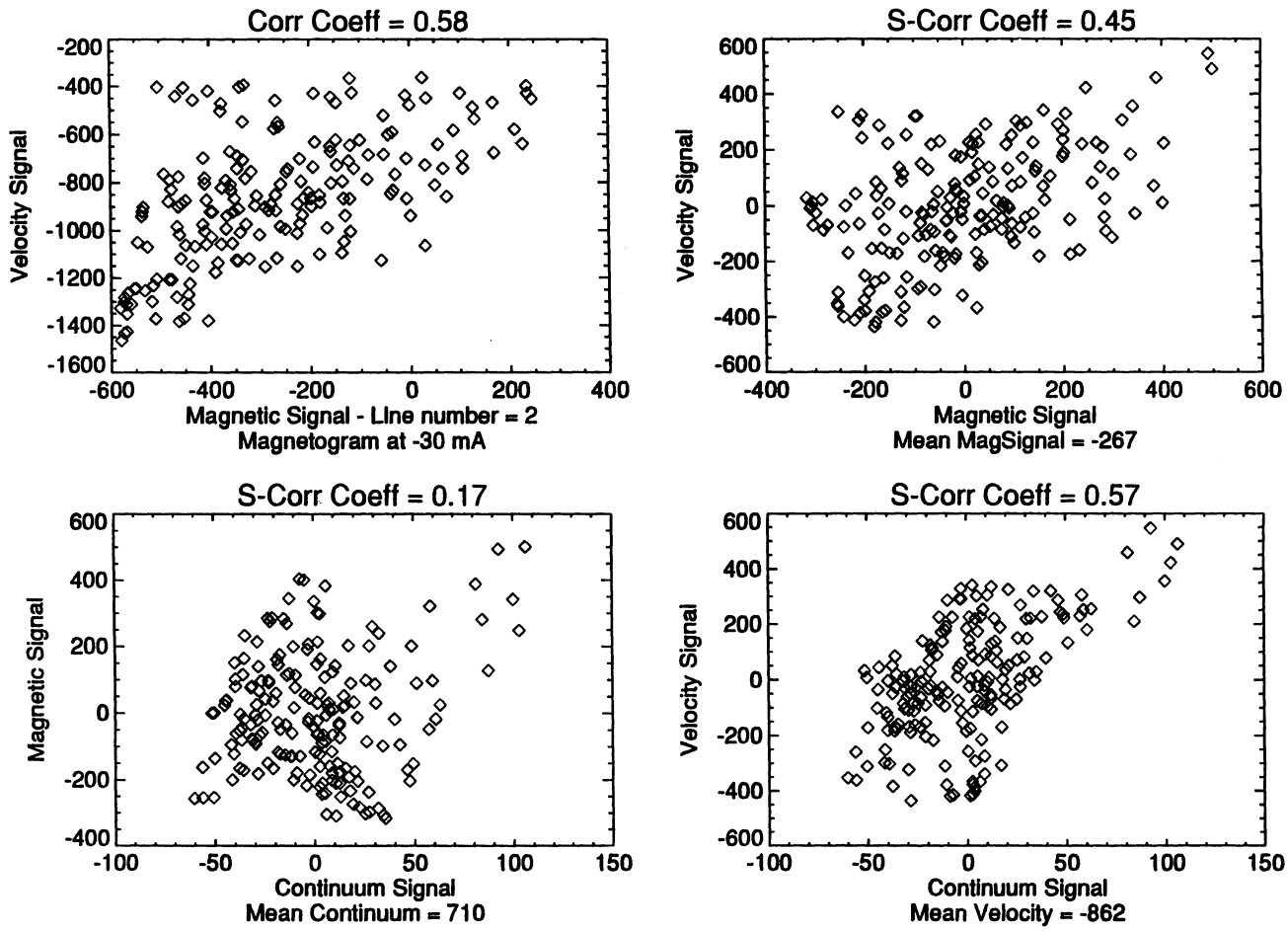

FIG. 13.—Panels from upper left to lower right display scatter plots of pairs of parameters for path 2. Immediately above each panel is the correlation coefficient and below the panel is the mean value of parameter. The upper left panel shows the data for the magnetogram and Doppler signal. The rest of panels show scatter plots for data with the third-order fit removed. From upper right to lower right are displayed magnetogram vs. Doppler, magnetogram vs. continuum, and Dopplergram vs. continuum.

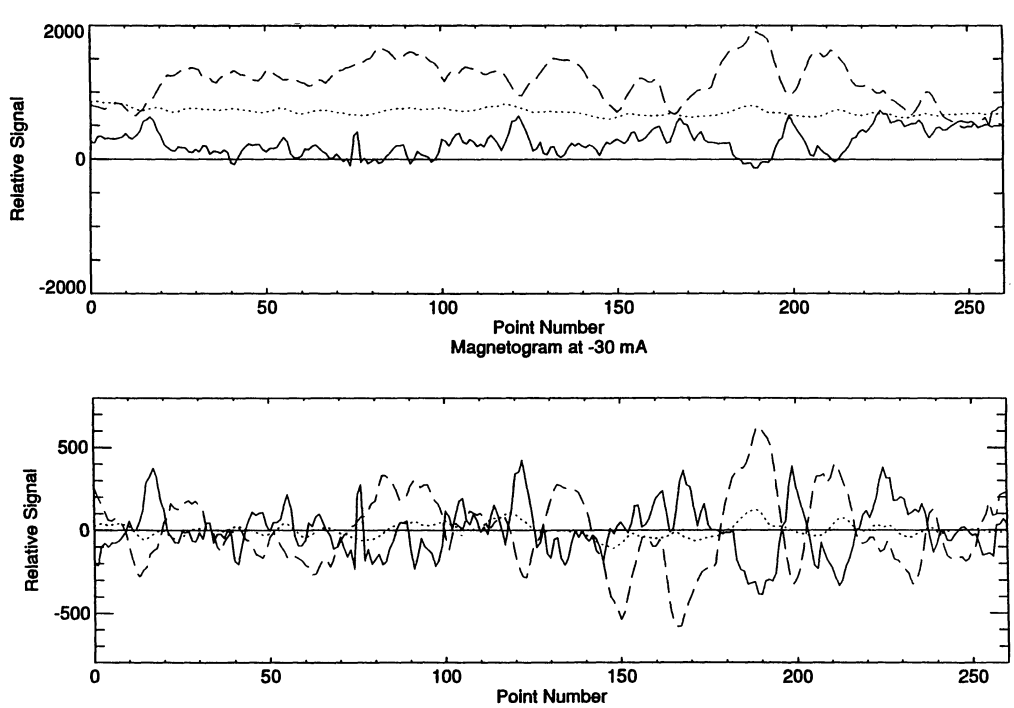

FIG. 14.—Same format as Fig. 12, but the data are from path 7

© American Astronomical Society • Provided by the NASA Astrophysics Data System

1993ApJ...403..780T

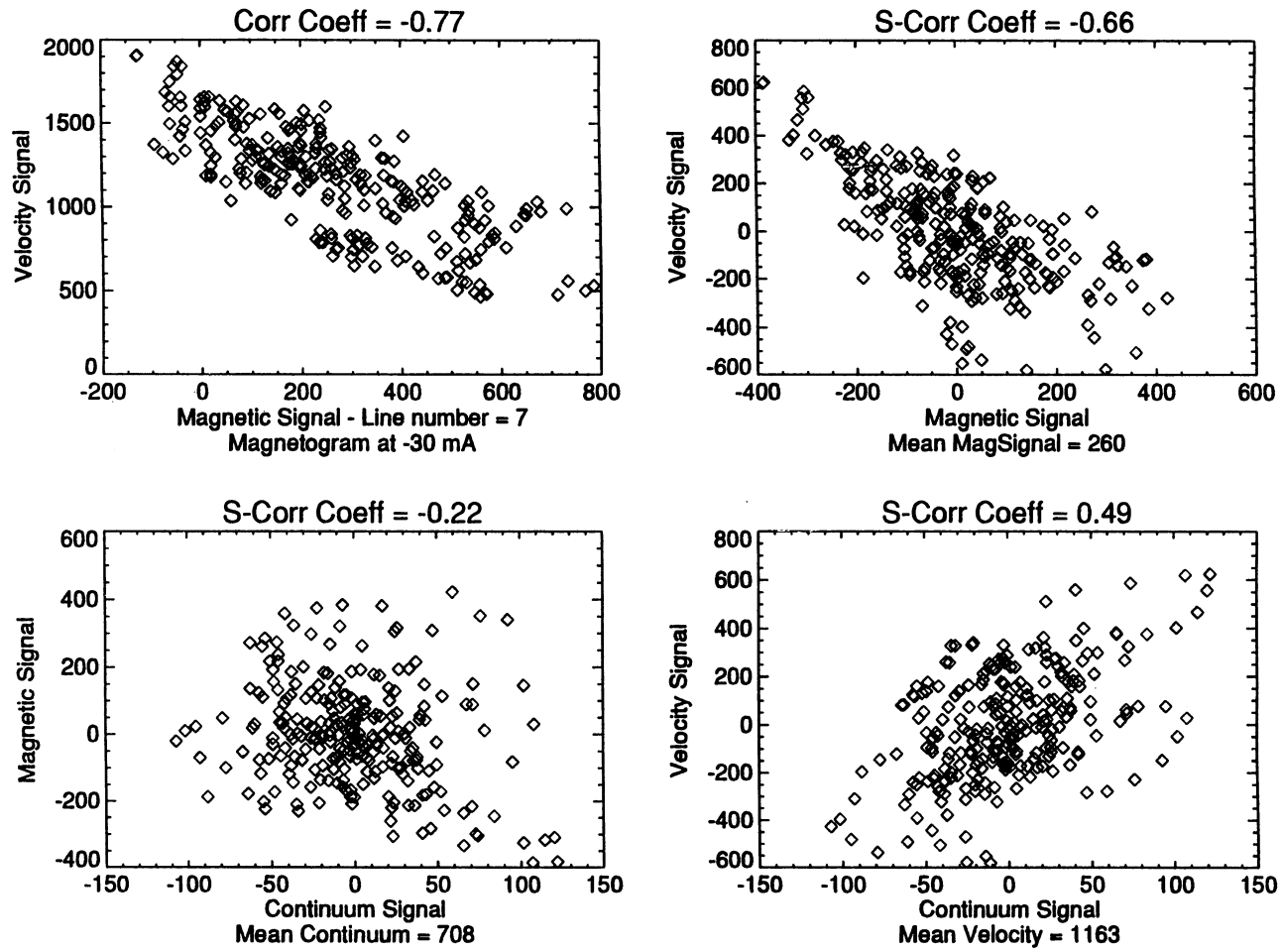

FIG. 15.—Same format as Fig. 13, but the data are from path 7

boundary on both sides of the spot. On the disk center side (limb) of the spot the magnetogram signal is positive (negative) in the −60 mÅ magnetogram. The outward Evershed flow in the magnetic field region shifts the disk center V-profiles to the blue, so that at mean line center the magnetogram signal becomes negative. On the limb side, the flow shifts the V-profiles red and also causes a negative signal magnetogram to appear at mean line center. Figure 16 illustrates the effect, the unshifted (*solid line*) and shifted (*dashed line*) V-profiles for the limbward and center disk sides of the spot are shown in the top and bottom panels, respectively.

The correlation between the detrended Dopplergram and continuum data is positive for all the paths. On the center paths this indicates that the higher speed flows occur in the darker continuum structures. While on the limb side, where the more horizontal flows have larger negative values, the positive correlation is also consistent with a correspondence between higher speeds and darker structures in the continuum. The correlation between the magnetogram and continuum data is usually small, an absolute magnitude of 0.2 or less, except near the umbra–penumbra boundary. The difference between the magnetogram and Dopplergram

TABLE 1

CORRELATIONS BETWEEN −30 mÅ MAGNETOGRAM, FOURIER DOPPLERGRAM, AND −750 mÅ CONTINUUM FILTERGRAM FOR LIMB (1–5) AND CENTER (6–11) PATHS

Number	M/V	S–M/V	S–M/C	S–C/V	Mean M	Mean V	Mean C
1	0.23	0.22	−0.02	0.13	−262	−917	783
2	0.58	0.45	0.17	0.57	−267	−862	710
3	0.34	0.44	0.24	0.40	−48	−673	702
4	0.22	0.44	0.13	0.12	291	−304	684
5	0.26	0.54	0.55	0.37	502	−144	671
6	−0.74	−0.75	0.06	0.02	244	1052	743
7	−0.77	−0.66	−0.02	0.49	260	1163	708
8	−0.62	−0.49	0.08	0.22	434	930	700
9	−0.50	−0.47	0.18	0.17	639	734	690
10	−0.52	−0.45	0.21	0.23	732	586	685
11	−0.05	−0.00	0.61	0.47	835	447	606

© American Astronomical Society • Provided by the NASA Astrophysics Data System

1993ApJ...403..780T

TABLE 2

−60 mÅ CORRELATIONS

Number	M/V	S–M/V	S–M/C	S–C/V	Mean M	Mean V	Mean C
1	0.19	0.20	−0.02	0.13	−260	−917	783
2	0.28	0.16	−0.06	0.57	−233	−862	710
3	0.35	0.54	0.19	0.40	−15	−673	702
4	0.30	0.60	−0.15	0.12	373	−304	684
5	0.25	0.44	0.32	0.37	874	−144	671
6	−0.52	−0.55	0.00	0.02	549	1052	743
7	−0.49	−0.33	0.11	0.49	690	1163	708
8	−0.43	−0.32	0.21	0.22	856	930	700
9	−0.37	−0.31	0.20	0.17	1122	734	690
10	−0.54	−0.47	−0.02	0.23	1432	586	685
11	−0.11	−0.04	0.66	0.47	1698	447	606

correlations with the continuum data may result because the flow field occurs largely in the dark continuum structures, while the magnetic field exists everywhere in the spot.

5. THE CURRENT SYSTEM OF SIMPLE FLUTED SUNSPOTS

In the sections above we have shown most of the variation in the magnetic signals result from inclination changes. In order to get an insight into the consequences of the observed geometry it is useful to examine how inclination variations modify the current distribution in the spot. To do this consider the effect of a sinusoidal perturbation in inclination with azimuth on a simple spot geometry. A cylindrically symmetric sunspot magnetic field configuration can be described in terms of a magnetic field strength, $B(r, z)$, and an inclination, $\gamma(r, z)$:

$$\boldsymbol{B}(r, z) = B(r, z)[\sin \gamma(r, z), 0, \cos \gamma(r, z)] , \tag{21}$$

where (r, ψ, z) indicates the components in the radial, azimuthal, and vertical directions.

Adding an azimuthal variation in only the inclination creates the more general form:

$$\boldsymbol{B}(r, \psi, z) = B(r, z)[\sin \gamma(r, \psi, z), 0, \cos \gamma(r, \psi, z)] . \tag{22}$$

Note that the magnitude of the magnetic field strength is independent of ψ.

Both equations (21) and (22) are subject to the condition $\nabla \cdot \boldsymbol{B}(r, \psi, z) = 0$.

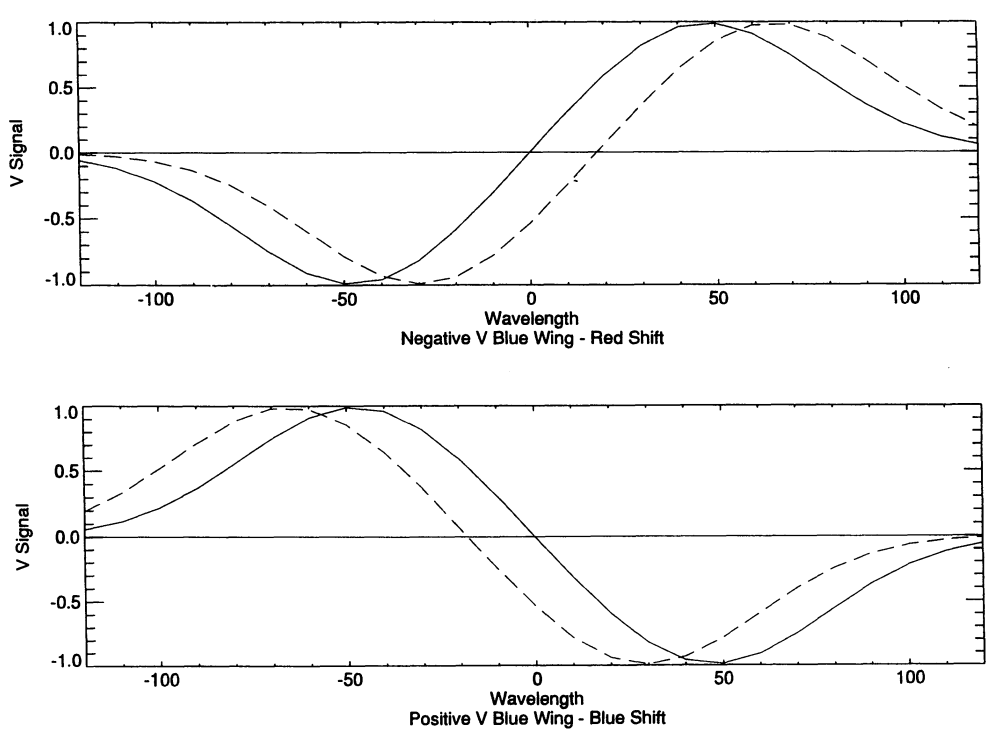

FIG. 16.—Shown are model plots of V-profiles for the limb (*top*) and disk center (*bottom*) sides of the spot ($B = 1$ kG, $V = 0.9$ km s^{-1}). The dashed curve in the top (bottom) panel is shifted to the red (blue) to simulate the limbward (disk center) flow caused by the Evershed flow. The solid curves are the undisplaced V-profiles.

© American Astronomical Society • Provided by the NASA Astrophysics Data System

1993ApJ...403..780T

For a vector field of the form described by equation (22), the current, $(\nabla \times \boldsymbol{B}[r, \psi, z])/4\pi$, can be written as the sum of a meridional (a meridional vector has no ψ component) and azimuthal vector,

$$\boldsymbol{J}(r, \psi, z) = \boldsymbol{J}_{\text{meridional}}(r, \psi, z) + J_{\text{azimuthal}}(r, \psi, z)\hat{\boldsymbol{\psi}} , \tag{23}$$

then

$$\frac{4\pi \boldsymbol{J}_{\text{meridional}}(r, \psi, z)}{c} = -\frac{\boldsymbol{B}}{r}\frac{\partial\gamma(r, \psi, z)}{\partial\psi} . \tag{24}$$

The azimuthal current is

$$\frac{4\pi \boldsymbol{J}_{\text{azimuthal}}}{c} = B(r, z)\hat{\boldsymbol{\psi}}\left\{\sin\gamma(r, \psi, z)\left[\frac{1}{B(r, z)}\frac{\partial B(r, z)}{\partial z} + \frac{\partial\gamma(r, \psi, z)}{\partial r}\right] - \cos\gamma(r, \psi, z)\left[\frac{\partial\gamma(r, \psi, z)}{\partial z} - \frac{1}{B(r, z)}\frac{\partial B(r, z)}{\partial r}\right]\right\} . \tag{25}$$

From equation (24) the meridional current is parallel to the field lines and does not contribute to the Lorentz force $\boldsymbol{J} \times \boldsymbol{B}$. Thus, the azimuthal variation in the inclination of the field does not generate a azimuthal force field. In this geometry field aligned currents exist without twisted field lines. In general there will be a meridional force generated by the azimuthal current that could be balanced by gravitational forces and meridional pressure gradients.

With some definitions, equation (25) can be written in the simpler form

$$\frac{4\pi \boldsymbol{J}_{\text{azimuthal}}}{c} = C(r, \psi, z)B(r, z)\sin(\gamma - \phi)\hat{\boldsymbol{\psi}} , \tag{26}$$

where

$$C(r, \psi, z) = \left\{\left[\frac{1}{B(r, z)}\frac{\partial B(r, z)}{\partial z} + \frac{\partial\gamma(r, \psi, z)}{\partial r}\right]^2 + \left[\frac{1}{B(r, z)}\frac{\partial B(r, z)}{\partial r} - \frac{\partial\gamma(r, \psi, z)}{\partial z}\right]^2\right\}^{1/2} , \tag{27}$$

and

$$\phi(r, \phi, z) = \arctan\left\{\left[\frac{1}{B(r, z)}\frac{\partial B(r, z)}{\partial r} - \frac{\partial\gamma(r, \psi, z)}{\partial z}\right]\Big/\left[\frac{1}{B(r, z)}\frac{\partial B(r, z)}{\partial z} + \frac{\partial\gamma(r, \psi, z)}{\partial r}\right]\right\} . \tag{28}$$

Let us assume that the inclination variation is a perturbation to an original field configuration of the form

$$\gamma(r, \psi, z) = \gamma_0(r, z) + \delta\gamma_n(r, z)\cos(n\psi) , \tag{29}$$

where $\gamma_n(r, z)$ is the amplitude of a cosinusoidal azimuthal perturbation with a period n and $\gamma_0(r, z)$ is the cylindrically symmetric component of the inclination. For this situation the force-free current is

$$\frac{4\pi J_{\text{meridional}}}{c} = -\frac{n\delta\gamma_n(r, z)\sin(n\psi)}{r}B(r, \psi, z) . \tag{30}$$

It is easy to understand the form of this current system. When the argument of the sine function is an odd multiple of $\pi/2$, the current is maximal and the perturbation term in the inclination is zero, so that

$$\gamma\left[r, \frac{(2j+1)}{2}\pi, z\right] = \gamma_0(r, z) , \tag{31}$$

where j is an integer. Hence, the maximal currents flow along undisplaced field lines and have a value

$$\frac{4\pi J_{\max}}{c} = \frac{(-1)^{(2j+1)}n\delta\gamma_n(r, z)}{r}B(r, \psi, z) , \tag{32}$$

At even multiples of π, the field inclination is at local extrema and the current is zero, and from equation (30) the current reverses at alternate zero crossings of the perturbation.

Using a value of 1500 G for the mean field of the spot, an umbral radius of 10″, and penumbral radius of 20″, a thickness of 1000 km, and 100 fibrils with an inclination variation amplitude of 20° the stored energy in the current system is about 10^{32} ergs.

A perturbation approach to the filamentary structure of sunspots has been examined earlier by Hu, Hu, & Low (1983) and Hu (1984) from a mathematical point of view. Their papers focused on showing that the field was stronger in the dark fibrils, but the methods suggested are powerful and revisiting the problem with the new experimental knowledge should prove very fruitful. Recently, B. C. Low (1989, 1991) has examined stability of force-free laminar magnetic structures in three dimensions. These laminar configurations have many of the characteristics of the fluted sunspot and are unusual in they can often be proved stable. There are no laminar solutions in a cylindrical coordinate system.

6. DISCUSSION

In summary, the measurements described above indicate the following:

1. There is a variation in inclination of the magnetic field in the penumbra of ± 15 to 20° with the spatial scale of the penumbral fibrils.

© American Astronomical Society • Provided by the NASA Astrophysics Data System

1993ApJ...403..780T

2. The magnetic field strength at a constant radius varies slowly compared to the spatial scale of the penumbral fibrils.
3. The average field inclination at the outer penumbral boundary is 70° to 75° to the sunspot normal.
4. The Evershed flow is on average more horizontal than the mean magnetic field at all radii in the penumbra.
5. The horizontal magnetic fields occur in the regions of the Evershed flow.
6. The Evershed flow is structured on the scale of the penumbral fibrils.
7. There is a tendency of the Evershed flow to occur in darker penumbral structures.
8. The magnetic field of the spot extends beyond the penumbral boundary.
9. The Evershed flow speed increases toward the edge of the penumbra and ends abruptly at the outer boundary of the penumbra.
10. There is a system of currents that are maximal along the edges of the penumbral fibrils.

These conclusions are summarized in a cartoon of a section of a spot shown in Figure 17 (Plate 8). In this schematic drawing sets of magnetic field lines near the umbral and penumbral boundaries are shown as colored inclined cylinders. The red and blue colors indicate current flow toward and away from the umbral, respectively. The color saturation indicates the magnitude of the flow.

In part to verify these results, Topka et al. (1991) have taken sequences of filtergrams in linear and circular polarizations and constructed line-of-sight, transverse field, and vector magnetograms of spots. They see fluctuations in both the line of sight and transverse fields that are consistent with results described above. In particular the patterns of fluctuations in the line of sight and transverse fields on the disk center and limb sides of a spot are consistent with the majority of the variation in magnetic signal being caused by inclination fluctuations. Keller, Stenflo, & von der Lühe (1991) using filtergrams taken simultaneously in right and left circular polarization in a Zeeman triplet have also seen fluctuations in the line-of-sight magnetic field on the scale of the penumbral fibrils. At the Vacuum Tower Telescope (VTT) on Tenerife in 1991 we have also taken filtergrams simultaneously in right and left circular polarization. Magnetograms made from these images look essentially identical to those made from sequential pairs. Schmidt et al. (1992) have analyzed these filtergrams and spectra taken simultaneously at the VTT and found that the magnetic field varies only slowly at a given radius and that the fluctuations in the longitudinal field are caused by inclination effects. Scharmer (1991) has very recently taken Stokes profiles with a spatial resolution approaching 0".3. He also reports that the line profiles indicate rapid changes in field inclination on the scale of penumbral fibrils.

From the body of measurements on sunspot fields, we conclude that the inclination variation of the magnetic field is great enough throughout the mid to outer penumbra to allow the more horizontal magnetic fields to be essentially parallel to the solar surface. This leads us to suggest that the Evershed flow occurs only in those magnetic field lines that are nearly parallel to the surface. The electric current calculations for a simple fluted sunspot suggest that the observed field inclinations do not require significant modifications to the concepts of force balance in spots in magnetostatic equilibrium.

In our data reduction we have not attempted to correct for either the telescope modulation transfer function or blurring in the Earth's atmosphere. We have also not considered the averaging processes that may occur in the solar atmosphere. These effects should act to lower the amount of observed inclinations variations, so that the actual inclinations in the solar atmosphere are probably somewhat greater than reported here.

It is very satisfying that our observations are consistent with the two apparently different views of the inclination of the magnetic field across a penumbra found in the literature. The original measurements of Hale et al. (1918) suggested that the magnetic field is nearly horizontal at the outer penumbral boundary. However, as pointed out in the section on the projection equations, we feel that the measurements described in the papers of Hale et al. (1918) and Hale & Nicholson (1938) were not made sufficiently close to disk center to accurately establish field inclinations at the outer penumbral boundary. Measurements using the location of the reversal line by Beckers & Schröter (1969) and Wittmann (1974) have more strongly supported the concept that the field was nearly horizontal at the outer penumbral boundary. In contrast the vector magnetic field observations of Adam (1971, 1975, 1990) and Lites & Skumanich (1990) have indicated that the field has a mean inclination of 70°–75° at the boundary of the spot with the photosphere. Detailed hydrostatic models of sunspots by Pizzo (1986, 1990) and Jahn (1989) yield stable configurations with field geometry not far from the potential field of a buried magnetic dipole, which implies field inclinations of 70°–75° at the outer penumbral boundary.

Kalman (1991) has reported on a very thorough study of the inclination of the vector magnetic field in the penumbra. Using vector magnetograph data from a number of sources, but with resolutions of about 3" or more, he concludes that the average inclination in the penumbra is 40° to 50° with respect to the vertical. However, the data also demand an rms error in the inclination measurements of 25° which results from "not only real measurement errors, but also effects of averaging within the magnetograph aperture ..." We conclude that the Kalman study is also consistent with a rapid fluctuation of the inclination angle in the penumbra. The existence of a range in inclinations at every radius in the penumbra creates a fundamental confusion for unresolved data.

During the last few years normal incidence X-ray telescopes have obtained very high-resolution images of the Sun. On the most recent flight of NIXT (Normal Incidence X-ray Telescope) one of the filters that reduce the visible light failed (Golub 1991). Because of the visible leak the location of X-ray loops with respect to a sunspot can be easily seen. Separate thin X-ray loops rise in the penumbra with inclination on the order 45°. The X-ray image suggests that the penumbral loops are coincident with the tops of the magnetic flutes.

To summarize we have shown that the mean inclination at the boundary is about 70°–75° in agreement with the Adam-Lites interpretation of the data, while the inclination fluctuations of $\pm 15°$–20° are sufficient to put a fraction of the field nearly horizontal, so that reversals are detectable on substantial segments of the penumbral boundary even near disk center, which can explain the results of Hale et al., Beckers and Schröter, and Wittmann. In addition, the observations seem to resolve the serious difficulty caused by the simultaneous existence of inclined magnetic fields and horizontal Evershed flows, while still allowing inclined fields in regions without Evershed flow. We note that Garcia de la Rosa (1987) suggested in a review of umbral and penumbral fine structures that a varying inclination of the penumbral fibrils was a reasonable explanation of a variety of penumbral features.

© American Astronomical Society • Provided by the NASA Astrophysics Data System

1993ApJ...403..780T

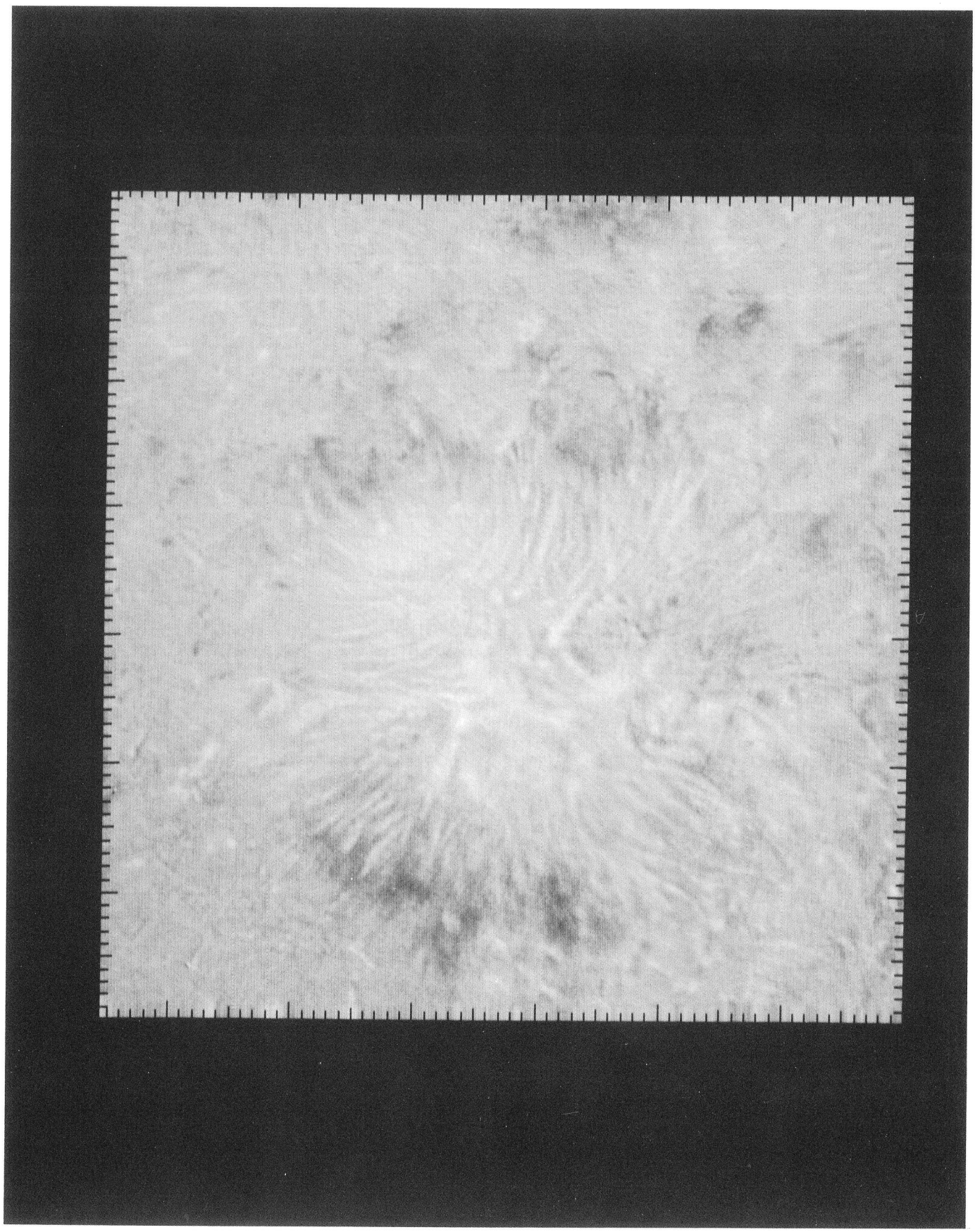

FIG. 10*c*

© American Astronomical Society • Provided by the NASA Astrophysics Data System

1993ApJ...403..780T

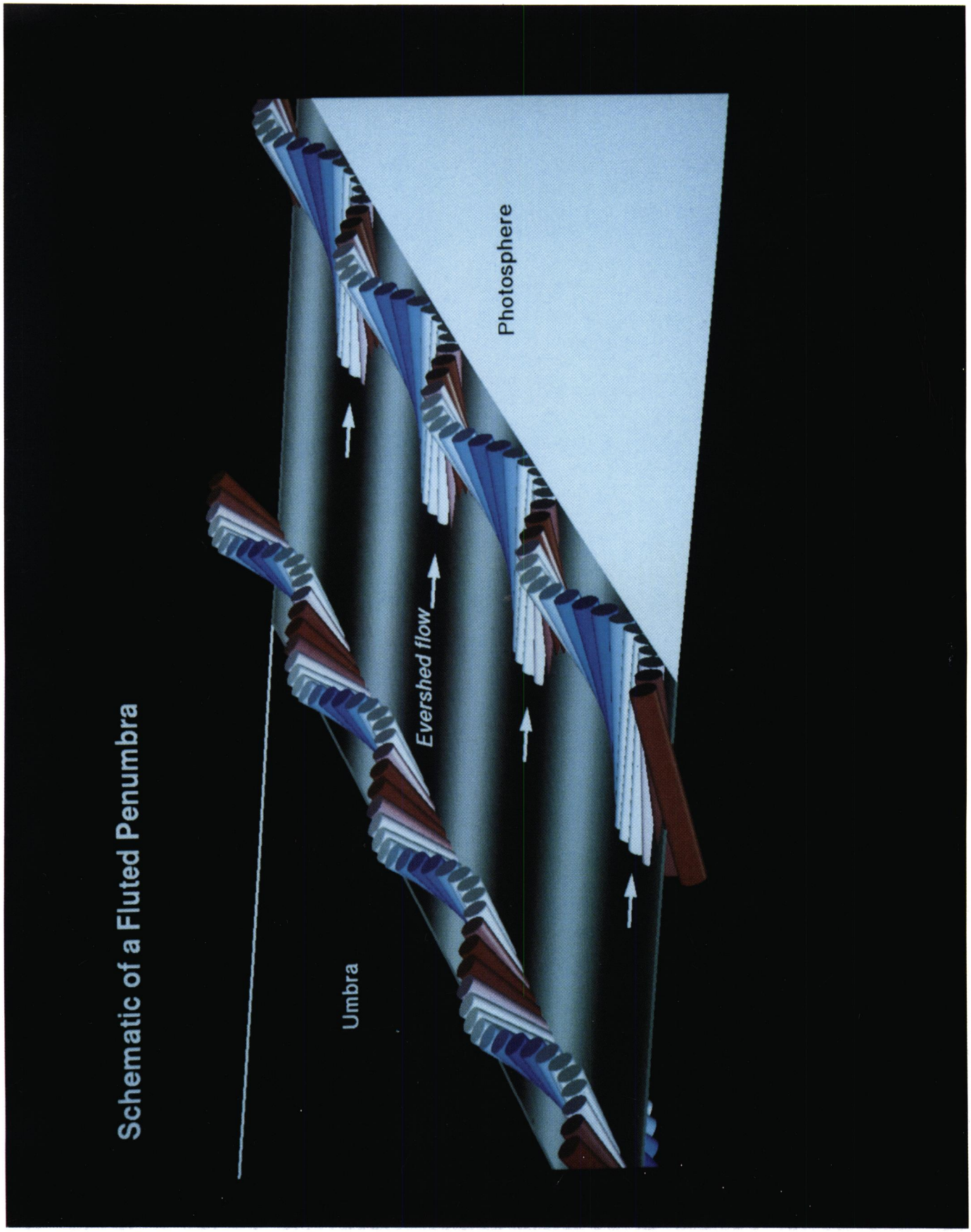

FIG. 17.—In this cartoon of a sunspot, sets of magnetic field lines near the umbral and penumbral boundaries are seen as colored inclined cylinders. The red and blue colors indicate current flow toward and away from the umbra, respectively. The color saturation indicates the magnitude of the flow. The bright and dark stripes in the penumbra indicate the dark and bright penumbral fibrils. The arrows indicate the location of the Evershed flow.

© American Astronomical Society • Provided by the NASA Astrophysics Data System

1993ApJ...403..780T

Although our measurements seem to be consistent with a relatively simple model in which the field lines vary in inclination around the spot being parallel to the surface in the darker fibrils and more inclined than a buried dipole field in the brighter ones, the picture completely neglects the possibility that the spot is an intrinsically dynamic phenomenon. Wentzel (1992) has suggested that the Evershed flow is the result of density fluctuations in magnetic flux bundles which causes them to fall toward the surface and flow outward along the bundle. Shine et al. (1990) have studied the Evershed flow in time sequences of Dopplergrams and have found that the flow tends to occur in moving clouds which are large compared to the penumbral fibrils. That is, a cloud represents a coordinated flow in adjacent fibrils. By tracking the motion of the clouds they measured velocities of 1.5 to 4 km s^{-1} which is consistent with their Doppler shifts. Time sequences of the Dopplergrams show the clouds are nonsteady with repetition rate of about 10 minutes. The path of the clouds tends to be coincident with dark fibrils and the fibrils tend to brighten during the passage of the clouds. The right penumbral structures do not have a detectable Doppler signature, although brightness fronts in them move toward the umbra with a velocity of about 300 m s^{-1}. Zirin & Wang (1991) have also observed flow fields in spots and their flow observations are consistent with those of Shine.

The development of the OSL evaluation tunable filter system represented a substantial effort of a team of hardware and software engineers and scientists at Lockheed Palo Alto Research Laboratory; we would especially like to acknowledge Mike Levay, Stuart Ferguson, Darrel Torgerson, Roger Rehse, Kathy Hwu, and Bill Rosenberg. The CCD camera, computer interface, and data acquisition computer were a joint effort of LPARL and the Kiepenheuer Institut für Sonnenphysik under the direction of Dexter Duncan, Chris Edwards, Mike Levay, and Thomas Rimmele. The logistics of the transportation and set up at the Swedish Solar Observatory was greatly aided by the efforts of Mike Morrill, Kermit Smith, Paco Armas, and Rolf Kever. We would like to especially thank Lennard Fisk, Bill Wagner, and David Bohlin of NASA Headquarters and Jerri Hartman and Daniel Spicer of Goddard Space Flight Center for their strong and continued support of scientific aspects of the engineering tests of the OSL evaluation system. We greatly appreciate helpful comments on data analysis made by Boon Chye Low, Piet Martens, Henk Spruit, Jack Thomas, Nigel Weiss, and Kees Zwaan. Financial support for this project was provided by NASA contracts NAS 8-32805 (SOUP) and NAS 5-26813 (OSL), by the National Science Foundation by grant ATM 8912841, the BMFT Förder Nr. 010E86059, the Swedish Royal Academy of Sciences, and Lockheed Independent Research.

REFERENCES

Adam, M. G. 1971, MNRAS, 145, 1
———. 1975, MNRAS, 155, 169
———. 1990, Solar Phys., 125, 37
Beckers, J. M., & Schröter, E. H. 1969, Solar Phys., 10, 384
Cram, L., & Thomas, J., eds. 1981, Observatory Conference, The Physics of Sunspots (Sunspot, NM: Sacramento Peak Obs.)
Evershed, J. 1909, MNRAS, 69, 454
Garcia de la Rosa, J. I. 1987, The Role of Fine-Scale Magnetic Fields on the Structure of the Solar Atmosphere, ed. H. Schröter, M. Vazquez, & A. A. Wyller (Cambridge: Cambridge Univ. Press), 136
Gokhale, M. H., & Zwaan, C. 1972, Solar Phys., 26, 52
Golub, L. 1991, Nature, 344, 6269, 842
Hale, G. E., Ellerman, F., Nicholson, S. B., & Joy, A. H. 1918, Contr. Mt. Wilson Obs., 165, 153
Hale, G. E., & Nicholson, S. B. 1938, Papers Mt. Wilson Obs., 5, Pt. 1, 1
Hu, W. R., Hu, Y. Q., & Low, B. C. 1983, Solar Phys., 83, 195
Hu, Y. Q. 1984, Chinese Astron. Astrophys., 8, 41
Jahn, K. 1989, A&A, 222, 264
Kalman, B. 1991, Solar Phys., 135, 299
Keller, C. U., Stenflow, J. O., & von der Lühe, O. 1993, A&A, submitted
Kinman, T. D. 1950, MNRAS, 112, 425
Lamb, S. A. 1975, MNRAS, 172, 205
Lites, B., Scharmer, G., & Skumanich, A. 1990, ApJ, 355, 329
Lites, B., & Skumanich, A. 1990, ApJ, 343, 747
Low, B. C. 1989, ApJ, 330, 992
———. 1991, ApJ, 370, 427
Maltby, P. 1964, Astrophys. Norvegica, 8, 205
November, L. J. 1986, Appl. Opt., 25, 392
Pizzo, V. J. 1986, ApJ, 302, 785
———. 1990, ApJ, 365, 764
Scharmer, G. B. 1989, in Solar and Stellar Granulation, ed. R. J. Rutten & G. Severino (Kluwer: Dordrecht), 161
———. 1991, private communication
Schmidt, W., Hofmann, A., Balthasar, H., Tarbell, T. D., & Frank, Z. A. 1992, A&A, in press
Schröter, E. H. 1971, in IAU Symp. 43, Solar Magnetic Fields, ed. R. Howard (NY: Springer), 167
Shine, R., Smith, K., Tarbell, T., & Title, A. 1990, BAAS, 22, 2, 878
Title, A. M., & Rosenberg, W. 1981, in Proceedings of the Sacramento Peak Observatory Conference, Solar Instrumentation: What's Next, ed. R. B. Dunn (Sunspot, NM: Sacramento Peak Obs.), 326
Title, A. M., Tarbell, T. D., Topka, K. P., Ferguson, S. H., & Shine, R. A. 1989, ApJ, 336, 475
Title, A. M., Topka, K. P., Tarbell, T. D., Schmidt, W., Balke, C., & Scharmer, G. B. 1992, ApJ, 393, 782
Topka, K. P., Frank, Z. A., Tarbell, T. D., Title, A. M., & Scharmer, G. 1991, BAAS, 23, 2, 1052
Topka, K. P., Tarbell, T. D., & Title, A. M. 1986, ApJ, 306, 304
Treanor, P. J. 1960, MNRAS, 120, 412
Wentzel, D. 1992, ApJ, 388, 211
Wittmann, A. 1974, Solar Phys., 36, 29
Zirin, H., & Wang, H. 1991, Adv. Space. Res., 11, (5), 231

© American Astronomical Society • Provided by the NASA Astrophysics Data System